**UNIVERSITÀ DEGLI STUDI DI CATANIA**

**DIPARTIMENTO DI INGEGNERIA ELETTRICA, ELETTRONICA ED INFORMATICA**

**Ph.D. course on "ENERGY**

**XXVI ciclo**

**EMANUELE DILETTOSO**

# EFFICIENT ELECTRO-THERMAL ANALYSIS AND OPTIMIZATION OF INDUCTION HEATING DEVICES

**Ph.D. THESIS**

Coordinatore:
Chiar.mo Prof. LUIGI MARLETTA

Tutor:
Chiar.mo Prof. NUNZIO SALERNO

# Contents

# INTRODUCTION

The use of eddy current devices is very common in several areas of Electrical Engineering such as non-destructive testing, electrical machines and induction heating. The latter, particularly, in the last decades, was widely applied to several fields, including heavy industry, chemical industry, electro-medical devices, domestic appliances. In fact this technique has a number of intrinsic advantages: such as a very quick response and a good efficiency. Induction heating also allows heating very locally, the heating speeds are extremely high because of the high power density and the heating process can be regulated precisely. The environmental impact is low, thanks to no production of flue gas and to the possibility to recover an important part of heat losses.

The aim of this work was the development of numerical methods for analysis and design of induction devices. The analysis of these devices is usually tackled by means of numerical techniques and can be often very hard due to the necessity to deal with a three-dimensional electromagnetic field problem that extends to infinity. In the case of an induction heating devices the electromagnetic analysis is coupled with a non linear thermal one. The proposed approach minimizes the computational cost of analysis with no loss of accuracy.

At first, a reduction of the number of numerical unknowns was obtained restrincting the FEM domain to conductors region by means of the new FEM-SDBCI method (Singular Dirichlet Boundary Condition Iteration), explained in Chapter I. The method is described for three-dimensional eddy current problems in which the electrical field is used as unknown in a mesh of edge elements. This method alleviates the major drawback of FEM-DBCI, that is, the insertion of some element layers between the integration and truncation surfaces and consequently allows the use of a common mesh for thermal analysis in coupled problems. The procedure couples a differential equation for the interior problem in terms of the electric field with an integral equation for the exterior one, which expresses the Dirichlet condition on the truncation boundary; note that, without the insertion of element layers between inner domain and truncation boundary, the integral equation becomes singular. The global algebraic system is efficiently solved in an iterative way. The use of an efficient mesh generator based on an artificial neural network which allows good-accuracy solutions with a lower computational effort is also described.

The generator grows an initial (moderately coarse) mesh of edge elements of tetrahedral shape up to a user-selected number of nodes. The mesh growth is driven by a node probability density function, which is obtained from an error estimation for the solution of the eddy current problem with the initial coarse mesh.

In Chapter II a strategy to perform FEM solutions of coupled electromagnetic-thermal problems is described. In this kind of problems, the electromagnetic one needs the large part of computing time; it is possible to limit the number of electromagnetic solutions by means of a control on the variations of temperature-dependent electric parameters. The solution of the eddy current problem leads to the calculation of power density in each finite element. Starting from this power density, a transient thermal analysis employing nodal tetrahedral finite elements of a given order is carried out. The thermal conductivity and the specific heat are assumed to be temperature-dependent. To solve the transient non linear problem, a Crank-Nicolson scheme was implemented.

In order to perform the design of induction devices the proposed analysis method was used as evaluation block into an optimization strategy particularly suitable to tackle this kind of problems, the PSALHE-EA algorithm, described in Chapter III. The PSALHE-EA has some new features that permit to considerably reduce the overall optimization time allowing to make full use of parallelization. Moreover, it is able to identify multiple optima by locating global as well as local optima; this aspect could be advantageous in industrial design, because the designer may want to see several design alternatives. The tests performed show that PSALHE-EA is a very efficient hybrid optimization method and in this work it was successfully applied to the design of an induction heater for conductor pieces.

Chapter I

# Electromagnetic Analysis of Induction Devices by means of the Singular FEM-DBCI Method

## 1.1 Introduction

In this chapter the Finite Element Method (FEM) is briefly introduced, with particular reference to its application to electromagnetic vector problems. Then an overview of the application of FEM-DBCI to the solution of time-harmonic eddy current problems in unbounded domains is given.

Subsequently, the application of FEM-SDBCI is explained in detail; finally numerical examples are given in order to validate the method.

## 1.2 Finite Element Method for open boundary electromagnetic problems

The FEM [1] is one of the most popular numerical methods for constructing approximate solutions to partial differential equations. The FEM is used by scientists and engineers to model the dynamic failure of structures, blood flow in the human heart, and thermal loads on electronic microchips, just to name a few applications. Originally developed by structural engineers, it is now widely applied in several fields and particularly to the numerical solution of electromagnetic Boundary Value Problems (BVP).

FEM is based on following main steps. The first step is subdivision of the problem domain into a set of subdomains (usually triangles or quadrangles in 2D, tetrahedra or parallelepipeds in 3D) called *finite elements (*triangles and tetrahedra are the most frequently used because of their greater adaptability); the union of all these elements is called a *mesh.* The second step is the translation of the BVP into a system of linear algebraic equations; the two most common ways to obtain this system are minimization of a functional related to the BVP and variational methods, such as the *Galerkin* weighted residual method.

In each element, the solution (e.g. the electromagnetic variable) is approximated by a set of simple position functions called *shape or basis functions*, The resulting (approximate) governing equations for elements are assembled into a global set of linear algebraic equations. The solution of this system of equations is followed by a post-processing stage in which the results are interpreted.

The repetition of local assembly to obtain a system of linear algebraic equations and the need to solve this usually sparse system by means of a numerical solver, lends itself to computer implementation, and in fact much of the success of the method parallels developments in computing science.

Let us now consider some aspects of FEM application to electromagnetic field problems. For three-dimensional problems in the time or frequency domain, it is generally necessary to employ a vector variable. With such a variable it is possible to perform the following nodal-based expansion (i.e. expansion using the same shape functions as (1.1)):

$$\vec{U}(\vec{r}) = \sum_{m=1}^{M} \vec{U}_m \alpha_m(\vec{r}) \tag{1.1}$$

where $\alpha(\vec{r})$ is a scalar shape function and$\vec{U}_m$ represents an array of $M$ unknown nodal vectors, that is to say 3$M$ scalars. The expansion (1.1) may be appropriate if the vector variable is one that can remain fully continuous throughout the problem domain, as is the case for vector potential $\vec{A}$ when employed in solving for eddy currents. On the other hand, if a field vector $\vec{E}$ or $\vec{H}$ is sought in regions with discontinuous material properties, there is a physical requirement for the normal vector component to be discontinuous at a material interface; otherwise, if a vector $\vec{D}$ or $\vec{B}$ is to be found, it is the tangential components which become discontinuous. In either case expansion

(1.1) is inappropriate and we must use a representation of the trial function $\vec{U}$, representing either $\vec{E}$ or $\vec{H}$, which conforms to these continuity rules. The working variable is then expanded using vector the interpolation functions $\vec{\tau}$:

$$\vec{U}(\vec{r}) = \sum_{m=1}^{M} U_m \vec{\tau}_m(\vec{r}) \tag{1.2}$$

defined within finite elements, where each $\vec{\tau}_m$ exhibits tangential but not normal continuity between elements.

By using tetrahedral elements for meshing 3D domains (Fig. 1-1), it is possible to associate a shape function $\vec{\tau}_m$ to every tetrahedron edge. Taking the inner product of functions $\vec{\tau}_m$ with tetrahedron edge vectors $\vec{e}_m$, *m=1,...6*, the following relations are satisfied:

$$\vec{e}_m \cdot \vec{\tau}_n = \delta_{mn} \tag{1.3}$$

where $\delta_{mn}$ is the Kronecker's symbol.

Thus if, in any given tetrahedral element a trial function $\vec{U}$ is represented by the edge interpolation functions:

$$\vec{U}(\vec{r}) = \sum_{m=1}^{6} U_m \vec{\tau}_m(\vec{r}) \tag{1.4}$$

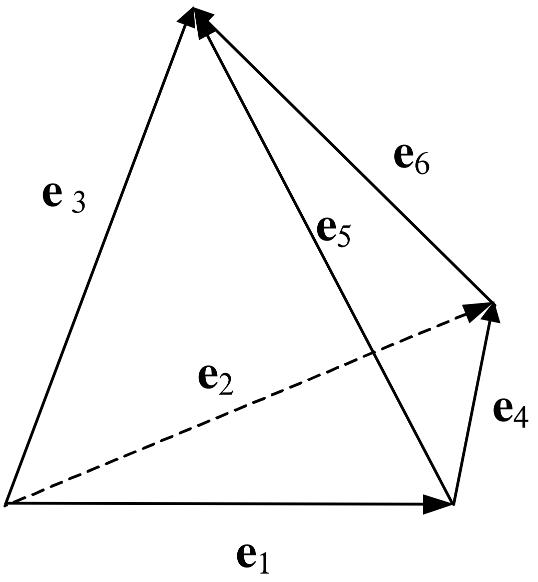

Fig. 1-1. Edge elements in a tetrahedron.

it is clear that the line integral of $\vec{U}$ along the tetrahedron edge $\vec{e}_m$ is

$$\int_{\vec{e}_m} \vec{U}(\vec{r}) \cdot d\vec{r} = U_m \cdot L_m \tag{1.5}$$

being $L_m$ the length of the edge, whilst the line integral along any continuous path of tetrahedron edges is just the algebraic sum of the appropriate *expansion coefficients* $U_m$ multiplied with the length of the path.

Practical electromagnetic problems often involve finding fields in infinite domains. Because of its nature, FEM cannot be applied to solve unbounded domain problems. The most brutal approach is to truncate the finite element mesh by means of sufficiently distant artificial boundary and impose approximate boundary conditions; generally, truncation introduces large errors into the solution and it requires an onerous computing effort. In order to solve unbounded domain problems using a finite-domain model, other techniques which solve the external field problem have to be coupled with the FEM. A great number of these methods are currently available for low or high frequency problems, with different degrees of computing effort and accuracy, e.g. the ballooning method, coordinate transformation, infinite elements, perfectly matched layer (PML) and hybrid methods such as FEM/BEM (Boundary Element Method).

## 1.3 3D Eddy current electric field formulation

Many different formulations are available to tackle this kind of problem, based on either fields or potentials, using one or more unknown variables [3-[5]. A convenient choice is to analyze an eddy current problem in a three-dimensional domain in terms of the electric field $\vec{E}$ [6]. The domain of a typical eddy current problem is shown in Fig. 1-2; the media are assumed to be linear, isotropic homogeneous and time-invariant; the boundary $\Gamma$ is, generally, constituted by two kinds of boundary: $\Gamma_E$ and $\Gamma_H$.

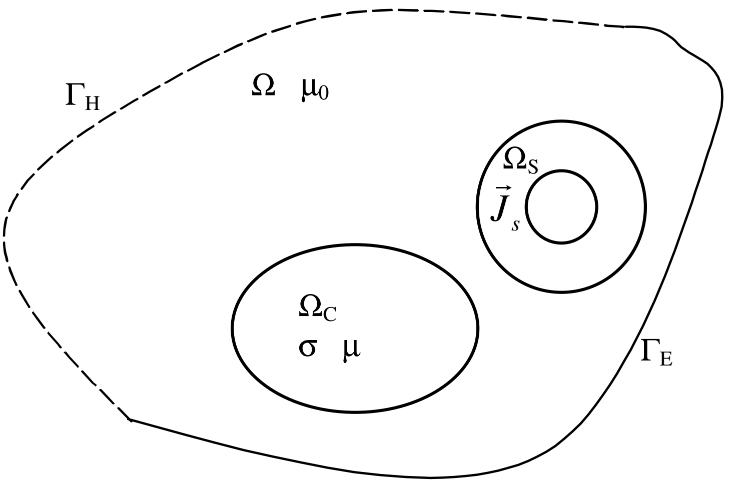

Fig. 1-2. Eddy current domain for electric field formulation.

At each point P on $\Gamma_E$ a Dirichlet boundary condition on the electric field $\vec{E} = \vec{E}_S$ is assigned:

$$\hat{n} \times \vec{E} = \hat{n} \times \vec{E}_S \qquad \forall \mathrm{P} \in \Gamma_E \tag{1.6}$$

At each point P on $\Gamma_H$ a Dirichlet boundary condition on the magnetic field $\vec{H} = \vec{H}_S$ is assigned

$$\hat{n} \times \vec{H} = \hat{n} \times \nabla \times \vec{E} = \hat{n} \times \vec{H}_S \qquad \forall \mathrm{P} \in \Gamma_H \tag{1.7}$$

Under the assumption of time–harmonic steady state behaviour, the system of Maxwell's equations can be rewritten as:

$$\nabla \cdot \vec{D} = \rho \tag{1.8}$$

$$\nabla \cdot \vec{B} = 0 \tag{1.9}$$

$$\nabla \times \vec{E} = -j\omega\vec{B} \tag{1.10}$$

$$\nabla \times \vec{H} = \vec{J} \tag{1.11}$$

where $\omega$ is the angular frequency.

The field vectors are related by the following material constitutive properties:

$$\vec{D} = \varepsilon\vec{E} \tag{1.12}$$

$$\vec{B} = \mu\vec{H} \tag{1.13}$$

where $\varepsilon$ and $\mu$ are the material permittivity and permeability, respectively.

The current density is related to the electric field and source currents by:

$$\vec{J} = \sigma\vec{E} + \vec{J}_s \tag{1.14}$$

where σ is the material conductivity.

The current continuity equation follows from (1.11) and is given by:

$$\nabla \cdot \vec{J} = 0 \tag{1.15}$$

Applying the curl operator to (1.10):

$$\nabla \times \frac{1}{\mu} \nabla \times \vec{E} = -j\omega\nabla \times \vec{H} \tag{1.16}$$

and by means of (1.11):

$$\nabla\times\frac{1}{\mu}\nabla\times\vec{E}=-j\omega\left(\sigma\vec{E}+\vec{J}_S\right) \tag{1.17}$$

Scalar multiplying (1.17) with a vector field $\vec{E}'$ called a test function, which satisfies homogeneous Dirichlet conditions on $\Gamma_E$, gives:

$$\frac{1}{\mu}\left(\nabla\times\nabla\times\vec{E}\right)\cdot\vec{E}'+\sigma j\omega\vec{E}\cdot\vec{E}'+j\omega\vec{J}_S\cdot\vec{E}'=0 \tag{1.18}$$

Applying the following vector identity

$$\left(\nabla\times\nabla\times\vec{E}\right)\cdot\vec{E}'=\nabla\times\vec{E}\cdot\nabla\times\vec{E}'+\nabla\cdot\left((\nabla\times\vec{E})\times\vec{E}'\right) \tag{1.19}$$

and integrating over domain $\Omega$, after application of Gauss theorem:

$$\begin{aligned}&\int_\Omega\frac{1}{\mu}\nabla\times\vec{E}\cdot\nabla\times\vec{E}'dV+\int_\Omega\sigma j\omega\vec{E}\cdot\vec{E}'dV=\\&\qquad=-\int_\Omega j\omega\vec{J}_S\cdot\vec{E}'dV-\int_\Gamma\frac{1}{\mu}\left((\nabla\times\vec{E})\times\vec{E}'\right)\cdot\hat{n}dS\end{aligned} \tag{1.20}$$

Let us examine the boundary term:

$$-\int_\Gamma\frac{1}{\mu}\left((\nabla\times\vec{E})\times\vec{E}'\right)\cdot\hat{n}dS=-\int_\Gamma\frac{1}{\mu}\left(\hat{n}\times\nabla\times\vec{E}\right)\cdot\vec{E}'dS \tag{1.21}$$

This integral can be subdivided into the two contributions on $\Gamma_E$ and $\Gamma_H$. Because on $\Gamma_E$ it is $\hat{n}\times\vec{E}^{'}=0$:

$$-\int_{\Gamma_E}\frac{1}{\mu}\left(\hat{n}\times\nabla\times\vec{E}\right)\cdot\vec{E}'dS=\int_{\Gamma_E}\frac{1}{\mu}\left(\hat{n}\times\vec{E}'\right)\cdot\nabla\times\vec{E}dS=0 \tag{1.22}$$

On boundary part $\Gamma_H$, using equations (1.7), (1.10) and the constitutive relation (1.13):

$$-\int_{\Gamma_H}\frac{1}{\mu}\left(\hat{n}\times\nabla\times\vec{E}\right)\cdot\vec{E}'dS=\int_{\Gamma_H}\left(\hat{n}\times j\omega\vec{H}_s\right)\cdot\vec{E}'dS \qquad (1.23)$$

The final integral equation in the electric field $\vec{E}$ is:

$$\begin{aligned}\int_{\Omega}\frac{1}{\mu}\nabla\times\vec{E}\cdot\nabla\times\vec{E}'dV+j\omega\int_{\Omega}\sigma\vec{E}\cdot\vec{E}'dV&=\\ =-j\omega\int_{\Omega}\vec{J}_S\cdot\vec{E}'dV+j\omega\int_{\Gamma_H}\left(\hat{n}\times\vec{H}_s\right)\cdot\vec{E}'dS\end{aligned} \qquad (1.24)$$

When the boundary conditions are only Dirichlet conditions on the electric field $\vec{E}$, (1.24) reduces to:

$$\int_{\Omega}\frac{1}{\mu}\nabla\times\vec{E}\cdot\nabla\times\vec{E}'dV+j\omega\int_{\Omega}\sigma\vec{E}\cdot\vec{E}'dV=-j\omega\int_{\Omega}\vec{J}_S\cdot\vec{E}'dV \qquad (1.25)$$

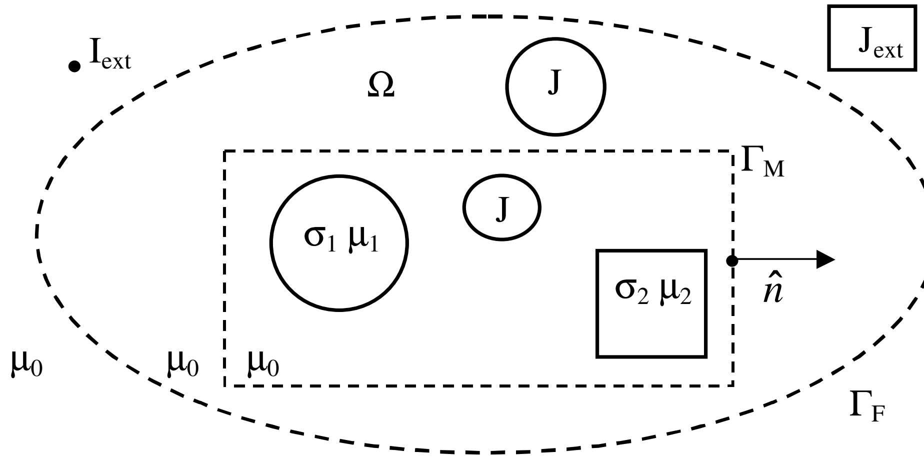

Fig. 1-3. Eddy current problem in open boundaries.

## 1.4 FEM-DBCI formulation

An unbounded three-dimensional domain of an eddy current problem is shown in Fig. 1-3. In order to apply FEM, the unbounded domain is truncated by means of a fictitious boundary $\Gamma_F$, enclosing all the eddy current conductors. Optionally some coils may be left outside of $\Gamma_F$. On $\Gamma_F$ a inhomogeneous vector Dirichlet boundary condition is assumed:

$$\hat{n} \times \vec{E} = \vec{E}_F \quad \text{on} \quad \Gamma_F \tag{1.26}$$

where $\hat{n}$ is the outward unit vector normal to $\Gamma_F$ and $\vec{E}_F$ is the unknown component of the electric field along the boundary.

Discretizing the bounded domain $\Omega$ delimited by $\Gamma_F$ by means of tetrahedral edge elements [7], the electric field is approximated in each tetrahedron as:

$$\vec{E} = \sum_{m=1}^{6} E_m \vec{w}_m \tag{1.27}$$

where $\vec{w}_m$ are first order vector shape functions:

$$\vec{w}_m = L_m(\varsigma_{1m}\nabla\varsigma_{2m} - \varsigma_{2m}\nabla\varsigma_{1m}) \tag{1.28}$$

with $\zeta_{1m}$ and $\zeta_{2m}$ the local coordinates in tetrahedron relative to the first and second node, respectively, of the edge $e_m$ and $L_m$ its length, and $E_\mathrm{m}$ is the expansion coefficient of the electric field defined as:

$$E_m = \frac{1}{L_m}\int_{\vec{e}_m} \vec{E}\cdot\hat{t}_m dl \qquad (1.29)$$

in which $\hat{t}_m$ is the unit vector along the edge.

Applying the Galerkin method and using the shape functions as weighting functions, the following matrix equation is derived:

$$\mathbf{AE}=\mathbf{B}_0 - \mathbf{A}_F\mathbf{E}_F \qquad (1.30)$$

where **A** and $\mathbf{A}_F$ are sparse FEM matrices, **E** and $\mathbf{E}_F$ are the arrays of the electric field expansion coefficients for the internal and boundary edges, respectively, and $\mathbf{B}_0$ is an array due to the source current.

Note that if some source coils are included in the analysis domain D, great care should be reserved to model the source current density in such a way that $\nabla\cdot\vec{J}_s = 0$ [8,9].

Equation (1.30) alone is not sufficient to solve the problem because it only allows **E** to be obtained once the correct $\mathbf{E}_F$ is known. If an incorrect guess is made for $\mathbf{E}_F$, the resulting **E** will be affected by a systematic error.

In order to solve the unbounded problem, it is thus necessary to derive another equation relating **E** to $\mathbf{E}_F$. This can be done by means Dirichlet Boundary Condition Iteration (DBCI) method [10-12]. The field on a point $P_F$ on $\Gamma_F$ can be expressed by means of the following integral equation [14]:

$$\vec{E}(P_F) = \vec{E}_{ext}(P_F) + \frac{1}{4\pi} \oint\!\!\!\oint_{\Gamma_M} \left( \frac{1}{r} \hat{n} \times \nabla \times \vec{E} + (\hat{n} \times \overline{E}) \times \nabla \frac{1}{r} + \hat{n} \cdot \vec{E} \nabla \frac{1}{r} \right) dS \qquad (1.31)$$

where $\Gamma_M$ is a closed surface enclosing all the eddy current conductors, but strictly enclosed by $\Gamma_F$ (see Fig. 1-3), $\hat{n}$ is the outward normal to $\Gamma_M$ at point P, $r$ is the distance between P and $P_F$, and $\vec{E}_{ext}$ is the electric field due to the coil source currents external to $\Gamma_M$. Substituting (1.31) in (1.29) for the edges on $\Gamma_F$ and expanding the field on $\Gamma_M$ as in (1.27), we obtain:

$$\mathbf{E}_F = \mathbf{E}_{ext} + \mathbf{HE} \qquad (1.32)$$

where **H** is a dense rectangular matrix in which null columns appear for the internal edges not involved in the computation. Note that since no singularities arise ($\Gamma_M$ and $\Gamma_F$ do not intersect each other) a simple Gauss integration can be used to evaluate the two integrals (that is, the surface integral on $\Gamma_M$ and the line integral on the generic edge of $\Gamma_F$).

A convenient approach to perform these computations is to select the surface $\Gamma_M$ as constituted by element faces, that is, triangles if tetrahedral elements are used. In this case, when the edge and the triangle are far apart, the Green function varies slowly so that a one-point quadrature is sufficient in both the triangle and the edge; when, on the contrary, the triangle and the edge are very close, the Green function varies rapidly due to the nearness of the singularity, and a large number of Gauss points is needed.

For tetrahedral edge elements, the integration accuracy can be selected according to the following rule. Let $L_M$ be the length of the longest edge of the triangle on $\Gamma_M$, $L_F$ the length of the edge on the fictitious boundary, L=$max(L_M,L_F)$ and $d$ the distance between their centers; then for $L/d \leq 0.2$ a one-point quadrature is used on both the triangle and the edge; for $0.2 \leq L/d \leq 1.1$ three Gauss points are used on the triangle and two points on the edge; otherwise six points are used on the triangle and three on the edge. This rule has proved to be a good tradeoff between accuracy and speed, as extensive numerical investigations have shown [15]. Of course this computation can be replaced by an FMM (fast multipole method) implementation of the integral equation (1.31) in order to reduce its computational complexity [17].

Combining (1.30) and (1.33) the global linear algebraic system of FEM-DBCI is formed:

$$\begin{bmatrix} \mathbf{A} & \mathbf{A}_F \\ -\mathbf{H} & \mathbf{I} \end{bmatrix} \begin{bmatrix} \mathbf{E} \\ \mathbf{E}_F \end{bmatrix} = \begin{bmatrix} \mathbf{B}_0 \\ \mathbf{E}_{ext} \end{bmatrix} \qquad (1.33)$$

where **I** is the identity matrix. The global system (1.33) allows solving the electromagnetic problem.

System 1.30 is similar to those arising from FEM-BEM methods, since it is made up of two parts: one comes from the differential equation and the other from the integral equation. However the diagonal submatrix related to the unknown on the fictitious boundary in (1.33) is the identity matrix, whereas in FEM-BEM this matrix is dense and nonsymmetric. The price paid for this advantage of FEM-DBCI is the introduction of an air gap between $\Gamma_F$ and $\Gamma_M$, which, however, can be selected as very thin (one or two layers of elements). Moreover, the adoption of a single vector unknown in both the conductors and air does not involve a significant increase in the computational cost with respect to other formulations employing a scalar potential in the air regions, since the air region can be set very small, by opportunely placing the fictitious boundary $\Gamma_F$ very near the conductor surfaces, which can be adopted as the integration surface $\Gamma_M$.

## 1.5 The FEM-SDBCI method

In order to alleviate the major drawback of FEM-DBCI, that is, the insertion of some element layers between the integration and truncation surfaces, this paper presents a modified version of the method, named FEM-SDBCI (Singular DBCI), in which the two surfaces are coincident, so that the integral equation becomes singular. In order to apply FEM, the unbounded medium is truncated by means of a fictitious boundary $\Gamma_F$, enclosing all the eddy current conductors (see Fig.1-4). Optionally some coils may be left outside. On $\Gamma_F$ a non-homogeneous vector Dirichlet boundary condition is assumed:

$$-\hat{n}\times\hat{n}\times\overline{E}=\overline{E}_F \qquad \text{on} \quad \Gamma_F \tag{1.34}$$

where $\hat{n}$ is the outward unit vector normal to $\Gamma_F$ and $\overline{E}_F$ is the unknown component of the electric field along the boundary.

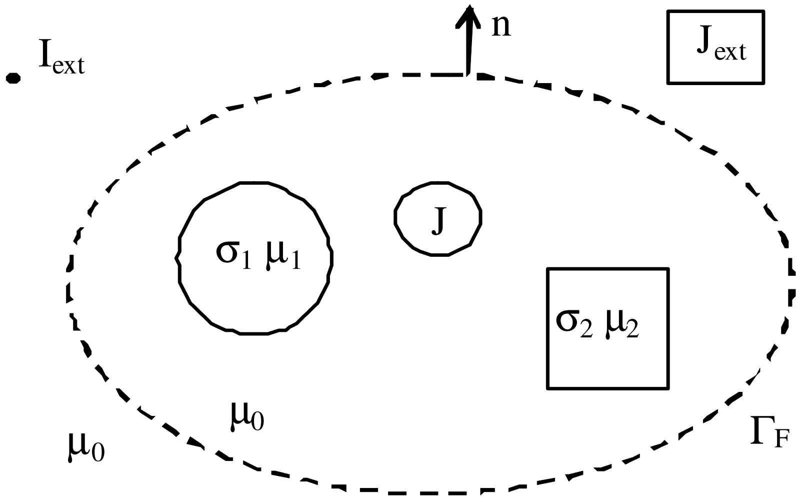

Fig. 1-4. Eddy current conductors and internal (distributed) source coils are enclosed by the fictitious truncation boundary $\Gamma_F$.

Applying the Galerkin method and using the vector shape functions as weighting functions, a matrix equation as in (1.34) is obtained.

In order to solve the problem, it is necessary to derive another equation relating **E** to $\mathbf{E_F}$. This can be done by expressing the field on a point $P_F$ on $\Gamma_F$ by means of the integral equation:

$$\frac{\alpha}{4\pi}\overline{E}(P_F) = \overline{E}_{ext}(P_F) + \frac{1}{4\pi}\oiint_{\Gamma_F}\left(\frac{1}{r}\hat{n}\times\nabla\times\overline{E} + (\hat{n}\times\overline{E})\times\nabla\frac{1}{r} + \hat{n}\cdot\overline{E}\nabla\frac{1}{r}\right)dS \tag{1.35}$$

where r is the distance between P and $P_F$, $\overline{E}_{ext}$ is the electric field due to the coil source currents external to $\mathbf{\Gamma_F}$, and $\alpha$ is the solid angle that $\mathbf{\Gamma_F}$ subtends at point $P_F$. The expansion coefficient $E_m$ relative to an edge $e_m$ lying on the fictitious boundary is expressed as:

$$\begin{aligned}\frac{\alpha}{4\pi}E_m &= \frac{1}{L_m}\int_{e_m}\overline{E}_{ext}(P_F)\cdot\hat{t}_m\,ds + \\ &+ \frac{1}{4\pi L_m}\sum_k\iint_{T_k}\int_{e_m}\left(\frac{1}{r}\hat{n}\times\nabla\times\overline{E} + (\hat{n}\times\overline{E})\times\nabla\frac{1}{r} + \hat{n}\cdot\overline{E}\nabla\frac{1}{r}\right)\cdot\hat{t}_m ds\,dS\end{aligned} \tag{1.36}$$

where $T_k$ is the k-th triangular patch on the fictitious boundary coming from the tetrahedral decomposition of the domain. In each patch the field is developed as in (1.27), where the six edges are those of the corresponding tetrahedron of which the patch constitutes one of its faces. Both the double integral on the triangle $T_k$ and the line integral on the edge $e_m$ are computed by means of the Gauss quadrature. The integration accuracy can be selected as in DBCI. The singularities arising in the integrand function in (1.29) are overcome by means of analytical formulas [22].

Consider a triangular patch $T_k$ of the fictitious boundary, relative to tetrahedron $E_k$ (see Fig. 1-5). A local coordinate frame is selected, in such a way that $T_k$ lies on the xy plane, vertex $V_0$ coincides with the origin and the other two vertices have coordinates $V_1=(x_1,0,0)$ and $V_2=(x_2,y_2,0)$. The fourth vertex of the tetrahedron $V_3=(x_3,y_3.z_3)$ has $z_3<0$; in this way the normal to the patch is $\hat{z}$. Assume that we want to evaluate the contribution of such patch to the mean value of the tangent component of the electrical field along its edge $V_0V_1$, whose versor is $\hat{x}$. The integration on such edge is performed by means of the Gauss quadrature method with Gauss points $P_n=(\xi_n x_1,0,0)$ $(0<\xi_n<1)$ and weights $w_n$, n=1,…,N. Then the second term in the right side of (1.36) is evaluated as:

$$\frac{1}{4\pi}\sum_{n=1}^{N} w_n \iint_{T_k}\left(\frac{1}{r}\hat{n}\times\nabla\times\overline{E}+(\hat{n}\times\overline{E})\times\nabla\frac{1}{r}+\hat{n}\cdot\overline{E}\nabla\frac{1}{r}\right)\cdot\hat{x}\,dS \tag{1.37}$$

where r the distance of the integration point $P=(x,y,0)\in T_k$ from the Gauss point $P_n$ on the edge. For each Gauss point $P_n$ it necessary calculate three integrals:

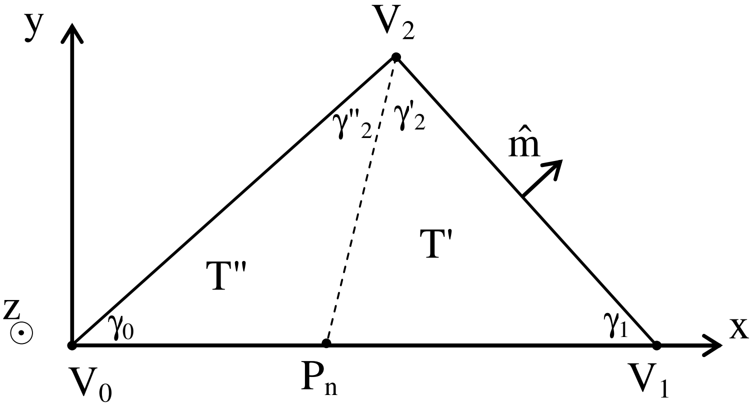

Fig. 1-5 Triangular patch on the fictitious boundary

$$I_1^{(n)} = \iint_{T_k} \left( \frac{1}{r} \hat{n} \times \nabla \times \overline{E} \right) \cdot \hat{x}\, dS \tag{1.38}$$

$$I_2^{(n)} = \iint_{T_k} (\hat{n} \times \overline{E}) \times \nabla \frac{1}{r} \cdot \hat{x}\, dS \tag{1.39}$$

$$I_3^{(n)} = \iint_{T_k} (\hat{n} \cdot \overline{E}) \nabla \frac{1}{r} \cdot \hat{x}\, dS \tag{1.40}$$

By noting that $\nabla \times \overline{E}$ is constant in the tetrahedron (and hence in the triangle), the first integral is simply computed by using the result:

$$\begin{aligned} I_0 = \iint_{T_k} \frac{1}{r} dxdy = x_1 \Bigg\{ & (1-\xi_n) \sin\gamma_1 \ln\left( tg\frac{\gamma_1}{2} tg\frac{\gamma'_2}{2} \right) + \\ & + \xi_n \sin\gamma_0 \ln\left( tg\frac{\gamma_0}{2} tg\frac{\gamma''_2}{2} \right) \Bigg\} \end{aligned} \tag{1.41}$$

The second integral vanishes since the normal to the triangle $\hat{n}$ $(=\hat{z})$ is orthogonal to ∇(1/r) which lies on the xy plane. The third integral leads to the calculation of

$$I = \iint_{T_k} (ax + by + c)\frac{\partial}{\partial x}\frac{1}{r}dxdy \tag{1.42}$$

where *a*, *b* and *c* are given coefficients; this integral is conveniently performed by subdividing the patch in two subtriangles T' and T'' (fig. 1-5):

$$\begin{aligned} I = {} & \frac{y_2}{e_0^2}\left[p_0(r_2 - r_1) + (ce_0 + ax_1e_0 - p_0r_1\cos\gamma_1)\ln q_0\right] + \\ & + \frac{y_2}{e_1^2}\left[p_1(r_2 - r_0) - (ce_1 - p_1r_0\cos\gamma_0)\ln q_1\right] - aI_0 \end{aligned} \tag{1.43}$$

where:

$$r_0 = \xi_n x_1 \tag{1.44}$$

$$r_1 = (1 - \xi_n)x_1 \tag{1.45}$$

$$e_0 = \sqrt{(x_2 - x_1)^2 + y_2^2} \tag{1.46}$$

$$e_1 = \sqrt{{x_2}^2 + y_2^2} \tag{1.47}$$

$$q_0 = \frac{e_0 + r_2 - r_1\cos\gamma_1}{r_1(1 - \cos\gamma_1)} \tag{1.48}$$

$$q_1 = \frac{e_1 + r_2 - r_0\cos\gamma_0}{r_0(1 - \cos\gamma_0)} \tag{1.49}$$

$$p_0 = a(x_2 - x_1) + by_2 \tag{1.50}$$

$$p_1 = ax_2 + by_2 \tag{1.51}$$

More details are given in Appendix A**.** Finally using the above formulas, (1.37) leads to:

$$\mathbf{HE}_{\mathrm{F}} = \mathbf{E}_{\mathrm{ext}} + \mathbf{GE} \tag{1.52}$$

where **H** and **G** are dense matrices. Matrix **H** is square by construction.

Combining ((1.30)) and (1.52) the global linear algebraic system of the FEM-SDBCI method is formed:

$$\begin{bmatrix} \mathbf{A} & \mathbf{A}_{\mathrm{F}} \\ -\mathbf{G} & \mathbf{H} \end{bmatrix} \begin{bmatrix} \mathbf{E} \\ \mathbf{E}_{\mathrm{F}} \end{bmatrix} = \begin{bmatrix} \mathbf{B}_0 \\ \mathbf{E}_{\mathrm{ext}} \end{bmatrix} \tag{1.53}$$

### 1.5.1 Solution of the FEM-DBCI global system

The global matrix in (1.53) is partly sparse, partly full and nonsymmetric. There is no efficient algorithm to solve this type of matrix equation. An iterative solver, which performs a matrix-vector multiplication at each iteration step, exhibits a complexity O(N) for the FEM part and $\mathrm{O}(\mathrm{N}_{\mathrm{F}}^2)$ for the integral part, where $\mathrm{N_F}$ is the number of edges on the fictitious boundary. Although $\mathrm{N_F}$<N, for large problems this approach is too onerous. The same complexity is exhibited by the approach in which (1.52) is substituted in (1.30) to yield the reduced system:

$$\left\lfloor \mathbf{A} + \mathbf{A}_{\mathrm{F}}\mathbf{H}^{-1}\mathbf{G} \right\rfloor \mathbf{E} = \mathbf{B}_0 - \mathbf{A}_{\mathrm{F}}\mathbf{H}^{-1}\mathbf{E}_{\mathrm{ext}} \tag{1.54}$$

It is clear from the above discussion that a good solving approach is one that only requires a few multiplications of the dense matrices **H** and **G** by vectors. This is obtained with the following two-block Gauss-Seidel iterative algorithm, which takes into account the very different nature of equations (1.30) and (1.52):

1) a first guess for $\mathbf{E}_{\mathrm{F}}$ is arbitrarily selected, for example $\mathbf{E}_{\mathrm{F}}=\mathbf{0}$;

2) equation (1.30) is solved for **E** by means of COCG;

3) the square matrix **H** is first decomposed into **L** and **U** matrices, and then equation (1.52) is solved for $\mathbf{E}_{\mathrm{F}}$;

4) at the generic n-th step, a convergence indicator is computed, measuring the distance between the new solution for $\mathbf{E}_{\mathrm{F}}$ and the old one:

$$\eta = 100\frac{\left\| \mathbf{E}_{\mathrm{F}}^{\mathrm{new}} - \mathbf{E}_{\mathrm{F}}^{\mathrm{old}} \right\|_2}{\left\| \mathbf{E}_{\mathrm{F}}^{\mathrm{new}} \right\|_2} \tag{1.55}$$

5) if convergence is not reached go to step 2, assuming a relaxed new guess for $\mathbf{E}_{\mathrm{F}}$ such as:

$$\mathbf{E}_{\mathrm{F}}^{(\mathrm{n})} = \gamma \mathbf{E}_{\mathrm{F}}^{\mathrm{new}} + (1-\gamma)\mathbf{E}_{\mathrm{F}}^{\mathrm{old}} \tag{1.56}$$

where $\gamma$ is the relaxation coefficient.

This iterative scheme exhibits the following characteristics:

a) since the first guess for the CG solver in each step is the solution obtained in the previous iteration step, the various solutions of system get faster as the iteration proceeds;

b) the LU decomposition is performed only once at the beginning of the iterative procedure; round-off errors in the LU decomposition are treated by selecting an appropriate (double precision) accuracy in the computing and storing of the matrices **H** and **G**.

c) the whole iterative procedure is convergent if an appropriate relaxation coefficient $\gamma$ is selected; this however is not known a priori; if a non appropriate coefficient $\gamma$ is used, divergence may occur;

d) consequently, the integral equation (1.52) is used only a few times, if compared to its use in an iterative CG-like solver for the whole non-symmetric system (1.53) or the reduced one (1.54).

By looking at the above iterative procedure more deeply, one realizes that the procedure can be interpreted as a stationary iterative method applied to the reduced system:

$$\mathbf{M}\,\mathbf{E}_{\mathrm{F}} = \mathbf{N} \tag{1.57}$$

where:

$$\mathbf{M} = \mathbf{H} + \mathbf{G}\mathbf{A}^{-1}\mathbf{A}_{\mathrm{F}} \tag{1.58}$$

$$\mathbf{N} = \mathbf{E}_{\mathrm{ext}} + \mathbf{G}\mathbf{A}^{-1}\mathbf{B}_0 \qquad (1.59)$$

Since it is well known that stationary methods are very weak and possibly non converging, one can think of finding a more robust substitute. The matrix **M** and vector **N** are not directly available. However, the vector **N** is simply built as follows:

1) assume a zero initial guess $\mathbf{E}_F=\mathbf{0}$;

2) solve the FEM equation ((1.30)) by means of the CG solver to obtain **E**;

3) compute $\mathbf{N}=\mathbf{E}_{ext}+\mathbf{GE}$, which coincides with the initial residual vector.

Similarly, matrix **M** can be used to perform matrix-vector multiplication $\mathbf{ME}_F$, as follows:

1) given the vector $\mathbf{E}_F$;

2) solve the FEM equation ((1.30)) with $\mathbf{B}_0=\mathbf{0}$ by means of the CG solver to obtain $\mathbf{E}=\mathbf{A}^{-1}\mathbf{A}_F\mathbf{E}_F$;

3) compute $\mathbf{ME}_F=\mathbf{HE}_F+\mathbf{GE}$.

Then non-stationary iterative CG-like solvers for non symmetric matrices, such as BiCG (BiConjugate Gradient), QMR (Quasi Minimal Residual), CGS (Conjugate Gradient Squared), BiCGstab (BiCG stabilized) and GMRES (all being polynomial accelerations of the Richardson method) can be used to solve (1.57).

Because the matrix-vector multiplications in this context are much more expensive than in a system where the coefficient matrix is directly available, GMRES should be preferred. In fact GMRES performs a true minimization of the residual and is thus the optimal method for accelerating the iterative solution of (1.55) as it minimizes the number of matrix-vector multiplications (neglecting the other operations required). The residual can be computed directly with the approximate solution, thus requiring a further matrix-vector multiplication, or by using the orthonormal basis of the Krylov subspace. The latter option is definitely preferable since matrix-vector multiplications are much more expensive than in a case where the coefficient matrix is directly available.

The major drawbacks of GMRES are the computing time and memory required to compute and store the orthonormal basis, which increases linearly with the number of iterations. So restarting procedures are often used. In our case the computing time and memory required for the orthonormal basis are only a small fraction of the total, because GMRES works on a reduced system, the number of unknowns being the values of the electric field along the edges of the fictitious boundary. Most of the computing time and memory is spent on solving (1.30), i.e. performing matrix-vector multiplications. It is therefore convenient to use long restarts which generally result in a full GMRES due to the quick convergence characteristic of the simple iterative procedure. The fact that the relaxed iterative procedure converges with a suitable choice of a positive relaxation parameter $\gamma$ indicates that the eigenvalues of the matrix **M** have positive real parts, and this assures that GMRES converges to the true solution even with a very short restarting parameter m.

In comparing the GMRES solving algorithm with the simple iterative one, it is to be noted that the GMRES solution does not require the LU decomposition of matrix **H**. This is a great advantage, especially for problems with large number of unknowns. Conversely, the various solutions of the FEM equations by means of the CG-solver are not related to each other, so the number of CG steps does not decrease as the solution proceeds.

## 1.6 An efficient Mesh Generator for Eddy Current Problems

Is is well known that the accuracy of the finite element solution depends on the discretization which is characterized by the finite element mesh and by the order of elements. In literature two main approaches exist to mesh a domain in order to apply the Finite Element Method (FEM) for the solution of a given field problem.

In the first approach the mesh is build in the preprocessing, before the solution of the problem [31]-[32]. In this approach the user expertise is extremely important: he should be able to foresee the domain parts in which to put more degrees of freedom (nodes or edges) and should utilize a suitable mesh generator, capable of such a fine specification. Meshes which are not very well optimized are therefore quite common.

In the second approach [33]-[37] the finite element mesh is adapted iteratively to the numerical solution, according to the following procedure: start with a coarse mesh, solve the field problem, estimate the solution error, refine the finite elements with greater errors, and iterate this process until a satisfactory accuracy is reached. This approach gives very accurate results, but a great computational effort is required. Moreover in some cases it is impractical, as for example in fast time-varying field problems. Other weak points of this approach are the fact that the user does not control exactly the degrees of freedom which he intends to invest for the solution of the problem and that the user expertise is not taken into account, so that a large percentage of computing time is spent on obtaining a mesh which could have been foreseen by an experienced user and from which the adaptation process could have been more conveniently started.

The tetrahedral mesh generator proposed in this work combines the two approaches by trying to take the best of each one. The mesh generator is based on an artificial neural network 101which grows an initial moderately coarse mesh of tetrahedral edge elements, according to a node probability density function (pdf), which is derived from an error analysis for the field solution computed with the initial mesh.

Let suppose to use a coarse mesh to solve the eddy current problem by means of SDBCI method; after the solution of (1.53) an error indicator $\eta_i$ is evaluated for the generic i-th tetrahedron in the mesh:

$$\eta_i = \frac{1}{N_a} \sum_{j=1}^{N_a} \left| E_{ij} - k_{ij} E_{ji} \right| \tag{1.60}$$

where the local index j refers to the $N_a$ adjacent tetrahedra ($1 \le N_a \le 4$), $E_{ij}$ and $E_{ji}$ are the normal components of the electric field evaluated in the barycentre of the triangular face in between the i-th and j-th tetrahedra by using the solution in the i-th tetrahedron and in the j-th one, respectively. In (1.60) the non dimensional coefficient $k_{ij}$ is defined as:

$$k_{ij} = \begin{cases} \sigma_j / \sigma_i & \text{if } \sigma_i \neq 0 \\ 1 & \text{if } \sigma_i = \sigma_j = 0 \\ 0 & \text{if } \sigma_i = 0 \text{ and } \sigma_j \neq 0 \text{ or viceversa} \end{cases} \tag{1.61}$$

where $\sigma_i$ and $\sigma_j$ are the electric conductivity of the two tetrahedra. Note that theoretically the exact solution should give $E_{ij}$-$k_{ij}E_{ji}$=0.

The node probability of the neural network generator is evaluated as

$$\pi_i = V_i \eta_i / \sum_{m=1}^{M_0} V_m \eta_m \qquad i=1,...,M_0 \tag{1.62}$$

where $V_i$ is the volume of the i-th tetrahedron and $M_0$ is the number of tetrahedra of the initial mesh.

The generation starts from the initial mesh of the domain by means of $M_0$ first-order tetrahedral finite elements. Its target is to add a number $N_{add}$ of additional nodes, as specified by the user. The initial mesh has two aims. First it defines the geometry of the domain D in which the FEM has to be applied. Secondly it constitutes the support of a piece-wise constant pdf f(**x**), $\mathbf{x} \in D$, by associating a probability $\pi_i$ that a node $\mathbf{x}_n$ of the final mesh lies in.

At the start of the generation the nodes and tetrahedra of the initial mesh are duplicated, so that the original ones are used to support f(**x**), $\mathbf{x} \in D$, and to search for of the node which best matches a given example point **x**, whereas the duplicated ones are used as the initial mesh to be manipulated by the generator. At the end of the generation the original nodes and tetrahedra are cancelled.

The generation is a stochastic process which can be seen as an ANN, similar to the Let-It-Grow neural network [35]. The learning phase of the neural network is based on a set of $N_{ex}$ example points, randomly derived from the pdf f(**x**). Each example point **x** is processed as explained in the following. First, the node $\mathbf{x}_h$ closest to $\mathbf{x}$ (best matching node) is selected and displaced toward $\mathbf{x}$ by:

$$\Delta\mathbf{x}_h = \alpha(\mathbf{x}-\mathbf{x}_h)+\beta(\mathbf{y}_h-\mathbf{x}_h) \tag{1.63}$$

where $\alpha$ and $\beta$ are parameters ($0\leq\alpha$, $\beta\leq1$) and $\mathbf{y}_h$ is the barycenter of the set of nodes $\mathbf{x}_k$ directly connected to node $\mathbf{x}_h$. If a node to be moved lies on the boundary surfaces or edges, only the component of the displacement along the same surface or edge is effectively taken into account. Nodes placed in the corners of the boundary are not moved at all. Once the best matching node $\mathbf{x}_h$ has been moved toward the example point $\mathbf{x}$, its error count $e_h$ is increased by one. No changes are made in the error counts of the neighbouring nodes $\mathbf{x}_k$.

Periodically in the learning phase (every $\xi=N_{ex}/N_{add}$ examples, $\xi$ being an integer parameter), a new node is inserted. The insertion procedure foresees the selection of the tetrahedron $T_m$ with the maximum error count $\varepsilon_m$, defined as the sum of the error counts of its nodes multiplied by a coefficient $1+\varphi f$, where $\varphi\geq0$ is a parameter and f is the number of boundary faces of the tetrahedron, the coefficient being introduced to favor the tetrahedra lying on the boundary. The new node is inserted in the barycentre of the longest edge of the tetrahedron $T_m$ (another coefficient $\psi$ $\geq0$ is utilized to favor the boundary and interface edges) and the original tetrahedron is refined. Of course all the other tetrahedra sharing that edge with $T_m$ are refined too.

Once a new node has been inserted, the error counts $e_n$ of the N nodes of the refined tetrahedra are decreased by a factor $\lambda(N-1)/N$, $(0\leq\lambda\leq 1)$, whereas the error count of the new node is initialized to $\mu/N$, $(0\leq\mu\leq 1)$ of the sum of the error counts $e_n$ of the nodes of the refined tetrahedra.

Once a certain amount of new nodes have been inserted, the mesh quality decreases, especially in the higher density regions, where bad-shaped tetrahedra appear, not allowing the further insertion of nodes. For this reason the Delaunay algorithm [31] is applied $N_D$ times in the growing process (every $\zeta=N_{ex}/N_D$ examples, $\zeta$ being an integer parameter).

When the number of nodes inserted reaches the user-specified value $N_{add}$, the learning algorithm stops. A final optimization of the mesh is performed based on the Delaunay algorithm and on moving the node towards the barycenter of its neighbors [31].

The various parameters of the generator have been optimized in [37]; the following values are used: $\alpha=0.030$, $\beta=0.016$, $\lambda=0.968$, $\mu=0$, $\varphi=0.20$, $\psi=1.40$, $\xi=10$, $\zeta=50$.

To measure the quality of the whole mesh, the mean, joint and minimum quality factors are employed:

$$Q_m=\frac{1}{M}\sum_{i=1}^{M}q_i \tag{1.64}$$

$$Q_j = M\left(\sum_{i=1}^{M} q_i^{-1}\right)^{-1} \tag{1.65}$$

$$q_{\min} = \min\{q_i\} \tag{1.66}$$

where

$$q_i=3r_i/R_i \tag{1.67}$$

is the quality of a single tetrahedron where $r_i$ and $R_i$ are the radii of the inscribed and circumscribed spheres, respectively.

## 1.7 Numerical examples

In this section a numerical example will be given to illustrate and validate the FEM-SDBCI method for 3-D eddy currents. The used finite element code is ELFIN [39].

### 1.7.1 The ELFIN code

The ELFIN code is written in Fortran. The basic features are N-dimensional (N=1,2,3) geometrical discretization, a wide application area, easy treatment of coupled problems, and a generalized iterative procedure. The ELFIN code is able to solve the following kinds of problems: Laplace, Poisson, Helmholtz, skin effect, motional diffusion and eddy currents.

The code is structured according to the classical scheme of FE codes, in which three distinct main programs are devoted to pre-processing, processing and post-processing, respectively. The pre-processing program (PREELFIN) exhibits a mixed interactive-batch user interface: in this part the user can define the geometric structure, the kind of problem, the materials and their properties, mesh generation, boundary conditions and sources. The processing program (ELFIN) works in a batch mode, starting from the data prepared in the pre-processing session and stored in a suitable file; the main aspects of the program are: generalized iteration structures, with four nested cycles (non-linearity, adaptive mesh refinement, boundary conditions, time discretization); numerical techniques (variational or Galerkin approaches are used), universal matrices and coupled problems. The post-processing program (POSTELFIN) exhibits the same interactive-batch user interface as the pre-processing one; available restitutions are displaying/printing of nodal values, 2D contour line plotting, axonometric 3D contour line plotting, and 2D and 3D vector plotting. Global quantities (energy, flux, current, etc.) can also be evaluated by means of integrals on elements, boundary (or local) sides or edges.

The most important feature that allows us to use ELFIN for the stochastic optimization of electromagnetic devices [40]**Errore. L'origine riferimento non è stata trovata.** is that the code uses symbolic variables as parameters (instead of fixed numeric values) of the batch input command files CMB and CMD of the pre- and postprocessing programs, respectively. The actual values of these parameters are given in the PCB file. In this way both the pre- and post-processing batch sessions (and so the whole code) can be made parametric with respect to a set of variables, typically representing the geometrical or constitutive data of the device to be optimized.

### 1.7.2 Bath Plate with two holes

An example is used to demonstrate the effectiveness of the FEM-SDBCI method. The system is the classical Bath plate with two holes [4],[41]. A conducting ladder ($\sigma$=32.78 MS/m) with two holes (length l=110 mm, width w=60 mm, height h=6.35 mm, central column and yoke width 10 mm, lateral column 20 mm) is under (s=15 mm) a toroidal coil (1260 Amp turns, frequency f=50 Hz) having a square section of side 20 mm, internal radius 20 mm and axis equations x =w/2, y =l/2+s (see Fig. 1-6). FEM-SDBCI was applied leaving the coil outside the fictitious boundary (which coincides with the conductor surface).

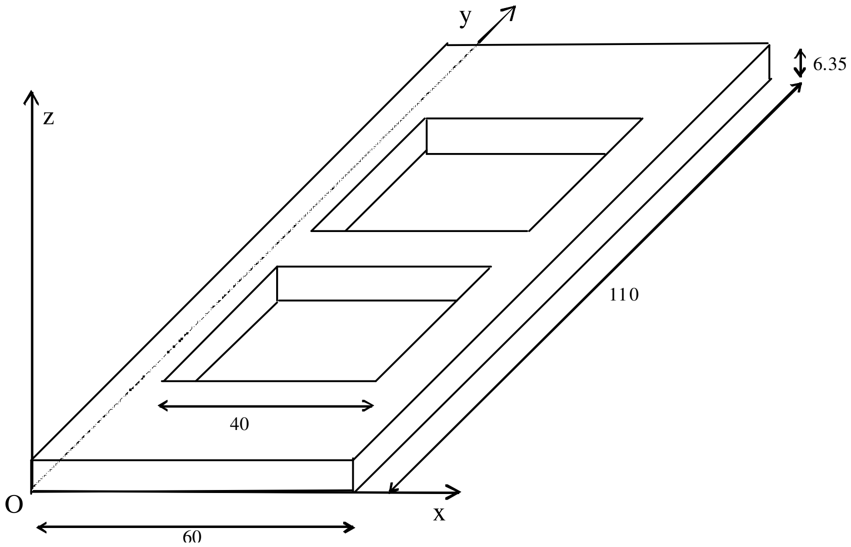

Fig. 1-6. Bath plate (dimension in mm).

The x=w/2 plane is a symmetry one, so only half of the original domain needs to be meshed, by imposing a homogeneous Dirichlet boundary condition on such a plane. Fig. 1-7 shows the initial mesh which consists of 657 nodes, 1680 tetrahedra and 2872 edges. The mesh was refined by means of the mesh generator of Par. 1.6. For the first solution the relaxed iterative scheme was used with $\gamma$=0.8. Starting from this solution the error indicators $\eta_i$ and the relative probabilities $\pi_i$ are computed. The artificial neural network mesh generator started with a target value of additional nodes $N_{add}$=1000.

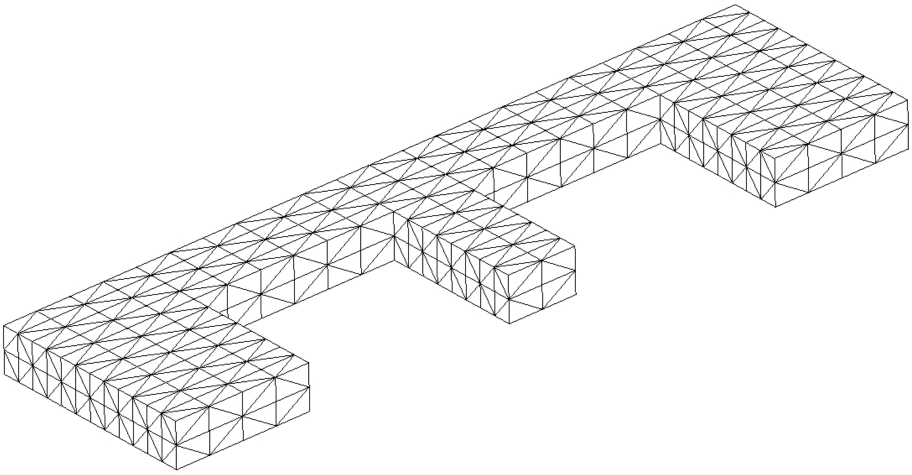

Fig. 1-7. Initial tetrahedral mesh of half ladder conductor.

Fig. 1-8 shows the obtained final mesh in the eddy current conductor. The whole mesh is constituted by 1657 nodes, 5143 tetrahedra and 8100 edges (4002 laying on the conductor's surface).

The mean, joint and minimum quality factors of the mesh are $Q_m$=0.722, $Q_j$=0.664 and $q_{min}$=0.043, respectively.

Fig. 1-12 reports the histogram of the quality factor $q_f$, as defined in (1.67), for ten classes, from 0.0-0.1 to 0.9-1.0.

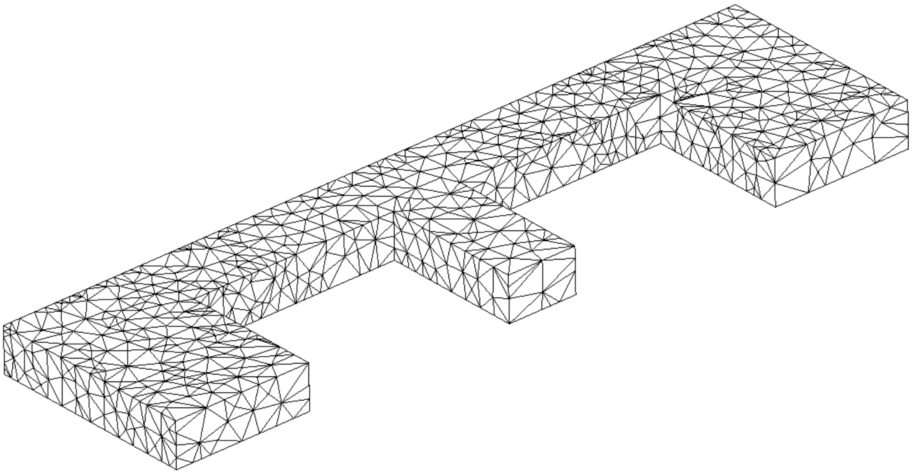

Fig. 1-8. Final tetrahedral mesh of half ladder conductor.

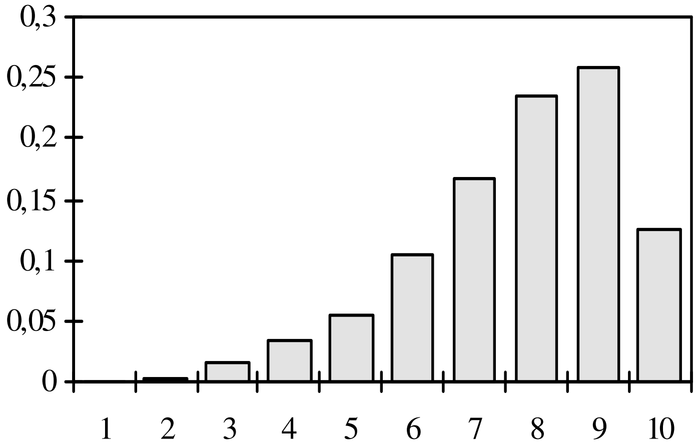

Fig. 1-9. Histogram of the quality factor $q_f$ for the final mesh.

Starting form the refined mesh, a new solution by means of SDBCI was obtained. The procedure reached convergence in 11 iteration steps with an end iteration tolerance of 0.1 per cent. Fig. 1-10 shows the eddy currents on the z=h/2 plane, whereas in Fig. 1-11 the Joule power density is drawn. A check of the Kirchhoff law was made by evaluating the three currents through the three sections with the symmetry plane: $I_1=I_2+I_3$; an acceptable fulfillment was obtained**.**

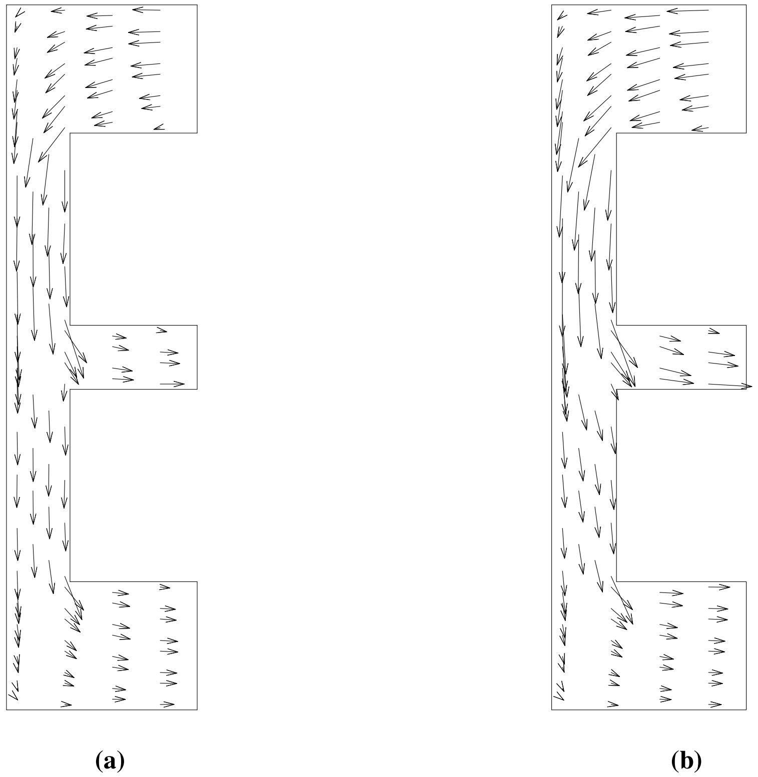

Fig. 1-10. – Real (a) and imaginary (b) parts of the eddy currents in the Bath plate.

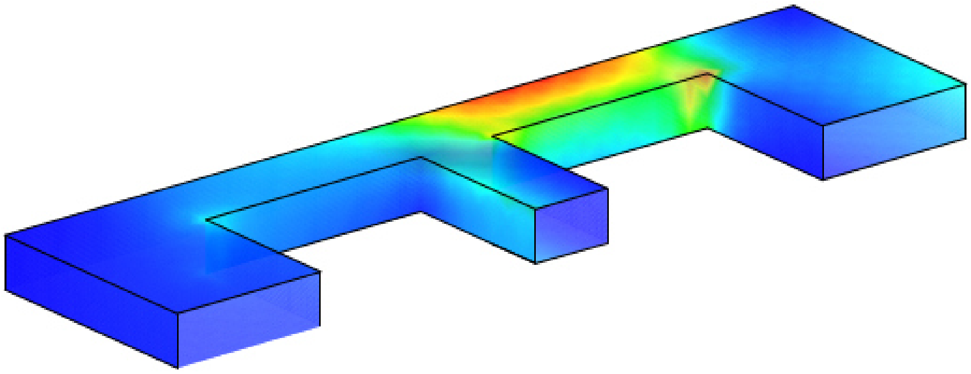

Fig. 1-11. Distribution of the Joule power density

Chapter II

# Coupled Electromagnetic-Thermal Analysis

## 2.1 Introduction

The analysis of induction heating devices is often very hard due to the necessity to deal with coupled three-dimensional electromagnetic field problems and non linear thermal coupled problems. However, both the problems can be tackled by means of the FEM method.

In this chapter FEM-SDBCI is applied to solve a coupled electro-thermal problem, in which a conductor is heated by means of eddy currents induced by time-harmonic source currents flowing in some coils. The solution thus obtained is used to compute the heating power density inside the conductor, from which a steady-state thermal analysis is performed by considering the same mesh, but employing nodal tetrahedral finite elements of a given order. The thermal conductivity is assumed to be temperature-dependent, as are the coefficients of the mixed boundary conditions on the surface of the conductor, which take radiation and convection into account. The thermal problem is therefore non-linear and is solved by a simple iterative procedure. The electric conductivity and magnetic reluctivity are also assumed to be time-dependent and so, although the electromagnetic problem is linear, another iterative procedure needs to be used to solve the coupled problem. In the following section method is described in detail.

## 2.2 Steady state coupled analysis

Once the eddy current problem has been solved, using the FEM-SDBCI method described in Chapter I, the heating power density in each finite element is computed as:

$$q = \frac{1}{2V}\iiint_V \sigma |E|^2 \,dxdydz = \frac{\sigma}{2V}\sum_{i=1}^{6}\sum_{j=1}^{6} E_i E_j^* t_{ij} \tag{2.1}$$

where V is the volume of the finite element, and $t_{ij}$ is the generic entry of the metric matrix, given by:

$$t_{ij} = \iiint_V \overline{w}_i \cdot \overline{w}_j \,dxdydz \tag{2.2}$$

Starting from the power density q the steady state thermal analysis can be performed by solving the Poisson differential equation

$$-\nabla \cdot (\kappa \nabla T) = q \tag{2.3}$$

where T is the temperature (in °C), $\kappa$ is the thermal conductivity (in W/m°C) and q is the heating power density (in W/m$^3$). Note that the thermal conductivity is a function of the temperature $\kappa(T)$, so that the thermal problem is non linear.

Another difficulty arises in the assignment of the boundary conditions on the surface of the heated piece. In this paper mixed conditions are assumed which take into account radiation and convection:

$$-\kappa\frac{\partial T}{\partial n}=(h_{rad}+h_{conv})(T-T_a) \tag{2.4}$$

where $T_a$ is the temperature of the surrounding fluid (air) and $h_{rad}$ and $h_{conv}$ are the coefficients of heat transfer due to radiation and convection, respectively. The coefficient $h_{rad}$ is evaluated as:

$$h_{rad}=\varepsilon\sigma(T_K+T_{Ka})(T_K^2+T_K T_{Ka}+T_{Ka}^2) \tag{2.5}$$

where $\varepsilon$ is the over-all interchange coefficient of the thermal radiation, $\sigma$=5.67·10$^{-8}$ W/m$^2$K is the Stefan-Boltzmann constant, and $T_K$=T+273.16 and $T_{Ka}$=$T_a$+273.16 are the absolute temperatures of the surface of the piece and of the surrounding fluid, respectively. The coefficient $\varepsilon$ depends on the material and the surface state of the piece.

Assuming a natural convection, the coefficient $h_{conv}$ is evaluated by means of the empirical relation:

$$\mathrm{Nu} = (\mathrm{Gr} \cdot \mathrm{Pr})^{(12+\log \mathrm{Gr}+\log \mathrm{Pr})/90} \qquad (2.6)$$

where Nu, Gr and Pr are the numbers of Nusselt, Grashof and Prandtl, respectively, given by:

$$\mathrm{Nu} = h_{\mathrm{conv}} d / \kappa_a \qquad (2.7)$$

$$\mathrm{Gr} = d^3 \rho^2 g \beta (T - T_a) / \mu^2 \qquad (2.8)$$

$$\mathrm{Pr} = c_p \mu / \kappa_a \qquad (2.9)$$

where d is a characteristic linear dimension of the piece, $\kappa_a$ the thermal conductivity of the air, $\rho$ the mass density, g the acceleration of gravity, $\beta$ the thermal expansion coefficient, $\mu$ the dynamic viscosity, and $c_p$ the isobaric specific heat. These quantity are evaluated at the temperature $T_a$, where appropriate. The coefficient $h_{conv}$ are further multiplied by 1.0, 1.2 or 0.5 according to the vertical, high horizontal or low horizontal orientation of the triangular side of the boundary of the piece.

As can be easily seen, all the coefficients appearing in the boundary condition are dependent of the temperature of the surface of the piece, so the problem and the relative FEM global system:

$$\mathbf{A}\,\mathbf{T} = \mathbf{Q} \qquad (2.10)$$

is nonlinear even if a temperature-independent thermal conductivity is assumed.

To solve this non linear problem, a simple iterative procedure has been implemented:

1) assume an initial uniform temperature distribution in the piece, for example $T=T_a$;

2) build the FEM global system by evaluating the thermal conductivity and the boundary condition coefficients at the given temperature distribution; to simplify this task, mean temperatures are computed for each tetrahedral finite element and for each triangular boundary side;

3) solve the FEM system for the new temperature distribution;

4) compute a convergence indicator $\eta$ of the 'distance' between the new and old temperature distributions, for example by means of:

$$\eta = 100\sqrt{\frac{\sum_n (T_n^{new} - T_n^{old})^2}{\sum_n (T_n^{new})^2}} \tag{2.11}$$

where the summations are extended to all the nodes of the finite element mesh;

5) if the indicator $\eta$ is lower than a prescribed tolerance $\eta_0$ the procedure is stopped; otherwise, assume the new temperature distribution as old (optionally by employing a relaxation coefficient $\gamma$) and go to step 2.

If the electric conductivity and magnetic reluctivity are also assumed to be temperature-dependent and so, another iterative procedure needs to be used to solve the coupled problem. The two analyses can be combined in the following iterative scheme:

a) assume an initial uniform temperature distribution in the heated conductor $T=T_a$;

b) evaluate the electrical conductivity $\sigma(T)$ and the magnetic reluctivity $\nu(T)$ on an element basis; build and solve the FEM-SDBCI global system (1.53) (note that only the matrix $\mathbf{A}$ changes with the temperature, whereas $\mathbf{B}_0$, $\mathbf{A}_F$, $\mathbf{G}$ and $\mathbf{H}$ do not); evaluate the heating power density q in each tetrahedron;

c) using the temperature distribution employed for the eddy current analysis as the starting temperature distribution, solve the nonlinear FEM system (2.10) to obtain a new temperature distribution;

d) check the convergence of the new temperature distribution with respect to that used in the last eddy current analysis; an indicator like that in (2.11) may be used; if convergence is not reached, go back to step b); otherwise stop the iterations.

## 2.3 Transient coupled analysis

Instead of steady state analysis, a transient thermal analysis can be executed, starting from the power density q calculeated after the first solution of eddy current prolem. The transient thermal analysis is performed by solving the differential equation

$$-\nabla\cdot(\kappa\nabla T)+c\rho\frac{\partial T}{\partial t}=q \qquad (2.12)$$

where T is the temperature (in °C) and κ is the thermal conductivity (in W/m°C), c is the specific heat (in J/kg °C) and ρ is the density (in kg/m$^3$). As in the previous paragraph, the thermal problem is non linear.

Applying the FEM to equation (2.12) with boundary conditions (2.4), the following non linear system of ordinary differential equations is built:

$$\mathbf{K}(\mathbf{T})\mathbf{T}+\mathbf{C}(\mathbf{T})\frac{d}{dt}\mathbf{T}=\mathbf{Q}(t)+\mathbf{B}(T) \qquad (2.13)$$

where **T** is the vector of the nodal values of the temperature, **K** and **C** are the temperature-dependent conductivity and capacity matrices, respectively, and **Q** and **B** are vectors depending on the power density and the boundary conditions (2.4), respectively.

To solve the transient non linear problem, (2.13), a Crank-Nicolson scheme was implemented [43] with a fixed time step Δt:

$$\mathbf{K}_{n+1/2}\mathbf{T}_{n+1/2}+\mathbf{C}_{n+1/2}\frac{1}{\Delta t}(\mathbf{T}_{n+1}-\mathbf{T}_n)=\mathbf{Q}_{n+1/2}+\mathbf{B}_{n+1/2} \tag{2.14}$$

Note that in FEM analysis the element sizes and the time step are very critical aspects. First, the elements have to be made small enough to yield sufficient information about the distribution of temperature. Next, a time step must be chosen that is sufficiently small, so that heat flow between elements can be approximated as a steady-state flow with little inaccuracy. A too large time step can introduce instability in the model. On the other hand, if the time step is too short, the computational cost increases with no gain in accuracy.

By approximating the matrices and the arrays as means of their values at the extremes of the n-th time step, we get:

$$\frac{1}{2}[\mathbf{K}_{n+1}+\mathbf{K}_n](\mathbf{T}_{n+1}+\mathbf{T}_n)+[\mathbf{C}_{n+1}+\mathbf{C}_n]\frac{1}{\Delta t}(\mathbf{T}_{n+1}-\mathbf{T}_n)=\mathbf{Q}_{n+1}+\mathbf{Q}_n+\mathbf{B}_{n+1}+\mathbf{I} \tag{2.15}$$

where:

$\mathbf{K}_{n+1}=\mathbf{K}(\mathbf{T}_{n+1})$ $\mathbf{K}_n=\mathbf{K}(\mathbf{T}_n)$ $\mathbf{C}_{n+1}=\mathbf{C}(\mathbf{T}_{n+1})$ $\mathbf{C}_n=\mathbf{C}(\mathbf{T}_n)$

$\mathbf{Q}_{n+1}=\mathbf{Q}(t_{n+1})$ $\mathbf{Q}_n=\mathbf{Q}(t_n)$ $\mathbf{B}_{n+1}=\mathbf{B}(\mathbf{T}_{n+1})$ $\mathbf{B}_n=\mathbf{B}(\mathbf{T}_n)$

Equation (2.15) is rewritten as a non linear algebraic system of equations:

$$\left\{\frac{1}{2}[\mathbf{K}_{n+1}+\mathbf{K}_n]+\frac{1}{\Delta t}[\mathbf{C}_{n+1}+\mathbf{C}_n]\right\}\mathbf{T}_{n+1}=\mathbf{Q}_{n+1}+\mathbf{Q}_n+\mathbf{B}_{n+1}+ \tag{2.16}$$

$$+\mathbf{B}_n+\left\{-\frac{1}{2}[\mathbf{K}_{n+1}+\mathbf{K}_n]+\frac{1}{\Delta t}[\mathbf{C}_{n+1}+\mathbf{C}_n]\right\}\mathbf{T}_n$$

The non linear system (2.16) is solved by a simple iterative procedure:

1) assume an initial temperature distribution in the piece =**T**$_{\mathrm{n}}$;
2) build the FEM global system by evaluating the thermal conductivity, the specific heat and the boundary condition coefficients at the two temperature distributions and **T**$_{\mathrm{n}}$; to simplify this task, mean temperatures are computed for each tetrahedral finite element and for each triangular boundary side;
3) solve the system for the new guess of temperature distribution **T**$_{\mathrm{n+1}}$;
4) compute a convergence indicator η of the 'distance' between the new and old temperature distributions, for example by means of:

$$\eta=100\frac{\left\|\mathbf{T}_{\mathrm{n+1}}^{\mathrm{new}}-\mathbf{T}_{\mathrm{n+1}}^{\mathrm{old}}\right\|_2}{\left\|\mathbf{T}_{\mathrm{n+1}}^{\mathrm{new}}\right\|_2} \tag{2.17}$$

5) if the indicator η is lower than a prescribed tolerance η0 the procedure is stopped; otherwise, assume the new temperature distribution as old (optionally by employing a relaxation coefficient γ) and go to step 2.

Note that this procedure is rapidly convergent, since the initial guess for $\mathbf{T}_{n+1}$ is very close to the solution.

The transient thermal analysis is combined with the time-harmonic eddy current analysis  in the following iterative scheme:

a) at time  t=0 assume an initial uniform temperature distribution in the heated conductor $T_0=T_a$; for each tetrahedral finite element evaluate the electric conductivity $\sigma(T_0)$ and the magnetic reluctivity $\nu(T_0)$; solve the eddy-current problem and evaluate the heating power density q;

b) start the transient thermal analysis to compute another temperature distribution $\mathbf{T}_1$ at time $t_1=\Delta t$;

c) continue the transient analysis, provided that the variations in the electrical conductivity $\sigma$ and magnetic reluctivity $\nu$ in each tetrahedron are lower than a given tolerance;

d) otherwise, for each tetrahedron recalculate the electric conductivity $\sigma$ and the magnetic reluctivity $\nu$, solve the eddy-current problem and evaluate the heating power density q; go to step c).

This combined iterative procedure is stopped when the time counter reaches the prescribed end-analysis value.

## 2.4 A numerical example

The example concerns the heating of a parallelepipedal piece, whose dimensions are 10 × 10 × 20 mm. The piece is made of aluminum and is surrounded by a concentric circular coil of rectangular cross section (internal radius 10 mm, external radius 12 mm, height 12 mm) which carries a total current $I_s$=2000 A at frequency f=100 Hz (see Fig 2-1).

The problem exhibits two symmetry planes so only 1/4 of the original domain needs to be meshed by imposing a homogeneous Dirichlet boundary condition on the xz and yz planes.

The eddy current analysis was performed by means of the FEM-SDBCI method.

A regular mesh of 2500 tetrahedral edge elements was employed with a total of 3705 edges (1340 laying on the cube surface). The procedure converged in 5 iterations assuming an end-iteration tolerance of 0.1 per cent for SDBCI and 0.01 per cent for the COGC solver.

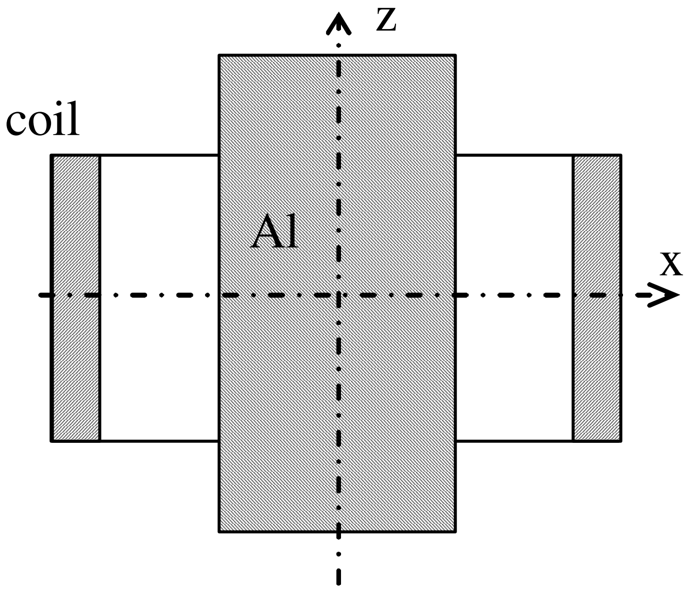

Fig 2-1: The system of the example: a parallelepipedal aluminum piece heated by a coil.

The analysis was performed using the following data:

- Aluminum electric conductivity:

$$\sigma(T) = \frac{37.74 \cdot 10^6}{1 + 3.9 \cdot 10^{-3}(T - T_a)} \tag{2.18}$$

- Aluminum thermal conductivity

$$\kappa(T) = 10.5 + \frac{189.73 \cdot T + 51826.65}{T - 209.836} \tag{2.19}$$

Aluminum specific heat $c(T_a)$ = 895 J/kg °C, emissivity $\varepsilon = 0.19$, characteristic dimension of the piece d=20mm, air temperature $T_a$ = 20 °C, air dynamic viscosity $\mu$ = 18.04 Ns/m$^2$, air thermal conductivity $\kappa_a$ = 0.026 W/m

°C, air isobaric specific heat $c_p$ = 1007 J/kg °C, air mass density: $\rho$ = 1.224 kg/m$^3$, air thermal expansion coefficient $\beta = 3.411 \cdot 10^{-3}$ K$^{-1}$.

In the thermal analysis the conductor was discretized by the same regular mesh of 2500 2nd-order tetrahedra and 4461 nodes. Homogeneous Neumann conditions were imposed on the xz and yz planes. The time step Δt was chosen equal to 10s. Assuming a tolerance of 1.0 per cent on the electrical conductivity changes, only 12 solutions of the electromagnetic problem were performed. Figure 2-2 the gives the values of the average temperature of the piece versus the time. Figure 2-3 shows the temperature distribution at final time.

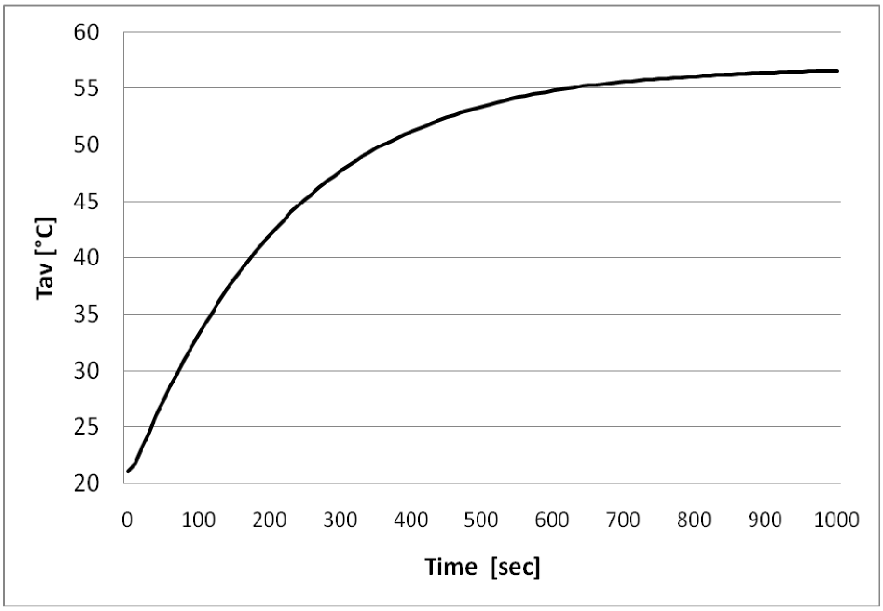

Fig. 2-2. Average temperature in the aluminum piece

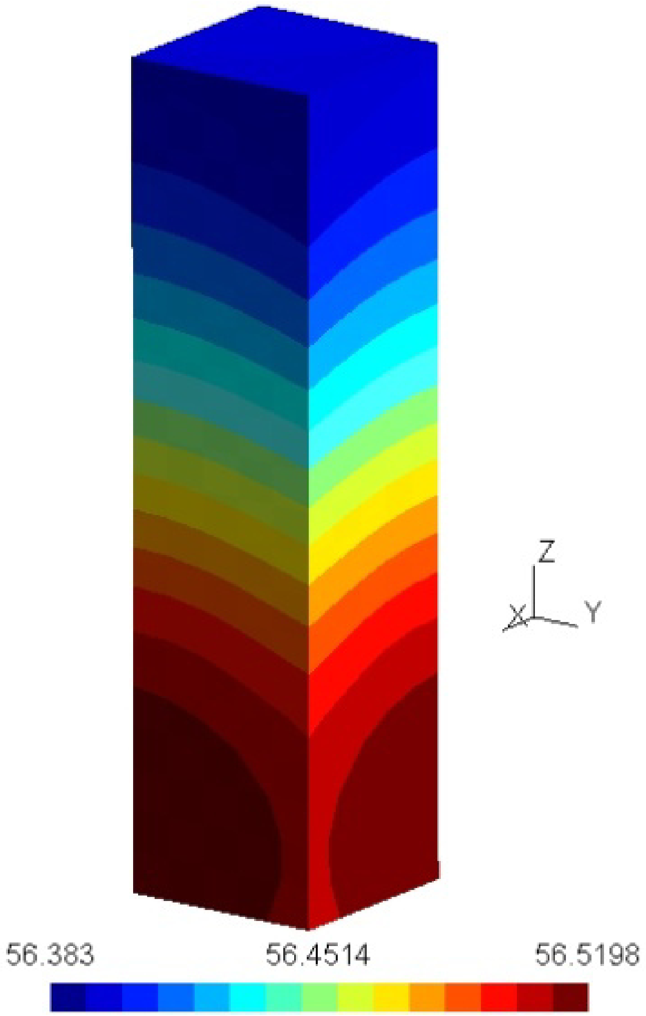

Fig. 2-3 Temperature distribution at time t=1000s

Chapter III

# Optimized design of an induction heating system by means of the PSALHE-EA algorithm

## 3.1 Introduction

Optimization techniques are often applied in engineering applications, like the design of electromagnetic devices. Often the devices have multiple specifications, i.e. it is necessary to employ multi-objective optimization methods. A more simple approach is to use a single objective function (OF) , obtained by means of the weighted sum of the objective functions related to each goal of the optimization problem. This weighted objective function is often multimodal, i.e. it presents multiple optima in the feasible domain. It is worth to note that by choosing the weights the designer restricts the search of multiple optima to one point on the Pareto front [45]. In this case, it may be helpful to provide to the designer not only the global optimum but even the local ones with their niche radius, giving useful information about the sensitivity of each optimum to decision parameters variations. This information, usually neglected by optimization algorithms that try to find the Pareto optimal front, is very important when a physical device or component is modeled.

The optimization of electromagnetic devices requires a method able to solve the optimization problem using only a few number of objective function evaluations. This is due to the high computational cost of a single evaluation; in fact it usually requires a solution by means of a numerical computational method: finite-element method, finite differences methid, method of moments and so on. Many EAs [45] such as Niching Genetic Algorithms (NGAs) [46] use niching techniques to maintain population diversity and to permit the investigation of many peaks at the same time, easily allowing the parallelization of the algorithm [47]. Sometimes these algorithms give their best performance with a high number of problem solutions. The reduction of the number of evaluations is an essential issue in electromagnetism. The SALHE-EA (Self-Adaptive Low-High Evaluation Evolutionary-Algorithm) [48] is an optimization method able to exploit the information given by all calculated solutions without neglecting poor solutions. In particular it is able to find multiple optima of a multimodal function and to give information about the fitness landscape in the neighborhood of these optima using a low number of solutions of the electromagnetic problem [52][53].

In this chapter an improved version of SALHE-EA is presented. This new version has some different features respect to the original one, that are: the number of individuals selected for reproduction each generation can be chosen by the user; each selected individual generates only one offspring; a replacement mechanism of the individuals that are identified as hypothetical maxima; the comparison mechanism applied to the fitness of parents and offspring after reproduction. These changes allow the full parallelization of the algorithm. The Parallel SALHE-EA (PSALHE-EA) is applied to the optimized design of induction eating device.

## 3.2 The SALHE-EA Algorithm

In the following optimization will refer to maximization without loss of generality. The SALHE-EA is a coupled stochastic-deterministic optimization algorithm. At the beginning of the stochastic section *N* individuals are random generated. After that, five fundamental steps are performed a fixed number of times *ng* (number of generations). These steps are: selection, mutation, elimination of useless individuals, identification of new hypothetical maxima (optima) and new hypothetical minima (they are “hypothetical” because they may differ from the true maxima or minima), evaluation of niche radii (the niche radius of an hypothetical maximum is the Euclidean distance from the closest hypothetical minimum).

At the end of the last generation the “doublets” are deleted. Doublets are the hypothetical maxima belonging to the same niche of another hypothetical maximum better of them. At the end of the stochastic section, a deterministic method, e.g. Pattern Search (PS) [49], is applied to the remaining hypothetical maxima in order to improve their OF value. The pseudo-code of SALHE-EA is shown in Fig. 3-1.

```
- begin
    - generates random population
    - do $n_g$ times
        - evaluation of fitness functions, $f_H$ and $f_L$, for each individual
        - selection
        - mutation
        - elimination of useless individuals
        - identification of new hypothetical maxima and
          new hypothetical minima
        - updating of niche radii
    - end do
    - deletion of doublets
    - starting of PS algorithm from each hypothetical maxima
    - updating of niche radii
    - deletion of doublets
- end
```

Fig. 3-1. Pseudo-code of SALHE evolutionary algorithm.

Let examine more in details the main steps of the algorithm.

In the selection step, in order to search for the maxima the value of $f_{Hi}$ of $i$-th individual depends on three factors: the value of the scalar objective function $f_i$, a penalization factor $\beta_i$ for the individuals present in crowded zones and a penalty factor $\rho_{Hi}$ for the individuals present in discovered niches.

$$f_{Hi} = (f_i)^{a_H} \beta_i^b (\rho_{Hi})^c \tag{3.1}$$

where $a_{H,}$ $b$ and $c$ are some scaling powers greater than or equal to one. The value of $\beta_i$ is calculated as follows:

$$\beta_i = \frac{d_i}{d_{\max}} \tag{3.2}$$

where $d_i$ is the average Euclidean distance between the $n_c$ individuals closest to the individual $i$ and $d_{max}$ is the largest $d_i$. Being $d_{ik}$ the Euclidean distance between individual $k$ and individual $i$, $d_i$ is calculated as follows

$$d_i = \frac{1}{n_c} \sum_{k=1}^{n_c} d_{ik} \tag{3.3}$$

Finally the penalty factor $\rho_{Hi}$ is defined as:

$$\rho_{Hi} = \prod_{j=1}^{m_H} \min\left(1; \frac{d_{ij}}{r_j}\right) \tag{3.4}$$

where $m_H$ is the number of niches, to which the individual $i$ belongs, $d_{ij}$ is the Euclidean distance between $i$ and the maximum in niche $j$ and $r_j$ is the radius of the niche $j$.

In order to search for the minima, a modified fitness $f_{i,L}$ is evaluated for the $i$-th individual in a similar way.

The niche radius $r_j$ is defined as the Euclidean distance in the design parameters space between a point of maximum $x_{jM}$ and its closest point of minimum $x_{jm}$:

$$r_j = \left\| \mathbf{x}_{jM} - \mathbf{x}_{jm} \right\| \tag{3.5}$$

The identification method of new maxima and minima is the following. An "hypothetical maximum" is an individual that, selected for reproduction, generates offspring with fitness values lower than its own for several consecutive times (parameter $nh$, chosen by user). Analogously an "hypothetical minimum" is an individual that generates, several consecutive times (parameter $nl$, chosen by user), offspring with fitness values higher than its own.

A individual $x_p$ selected by means of wheel one W1, generates an offspring $x_o$ by means of the mutation operator that adds a random vector to $x_p$. The value of the $k$-th parameter is computed as:

$$x_{o,k} = x_{p,k} + sign(r_1 - 0.5)\ r_2\ step_k \tag{3.6}$$

where $r_1$ and $r_2$ are [0,1] random numbers, and:

$$step_k = \frac{\Delta_k}{N} \sqrt{\frac{N}{n_k}} \left( 1 + \frac{1-\sqrt{n_k}}{\sqrt{n_k}} \frac{f_p - f_{\min}}{f_{\max} - f_{\min}} \right) \left( 2 - \rho_{Hp} \right)^e \tag{3.7}$$

where $N$ is the number of individuals in the population, $\Delta k$ is the domain of the $k$-th design parameter, $f_p$, $f_{min}$ and $f_{max}$ are the values of the scalar objective function for the parent, the worst and the best individual respectively. Considering N regular subdivisions of $\Delta k$, $n_k$ is the number of intervals in which at least one individual is present. Parameter $e$ is a scaling power greater than or equal to one. A similar mutation mechanism is applied to individuals selected by means of wheel W2. Equation (3.7) controls the balance between exploration of unknown zones of the search space and exploitation of attractive areas of the search space. If the number $N$ of individuals in the population is sufficiently large to explore the search space, the factor $\Delta k/N$ in (3.7) is small and forces new individuals to search locally. Otherwise the term $\Delta k/N$ is larger and the new individuals are spaced out, favoring exploration of the whole space. The second term in (3.7) preserves diversity in the population: if individuals tend to crowd, the number $n_k$ becomes small and $step_k$ goes up. The third factor in (3.7) also has an influence on the balance between exploration and exploitation, forcing individuals with high fitness values to search locally and individuals with low fitness values to search globally. Finally, the last factor in (3.7) increases $step_k$ if the parent belongs to a discovered niche: this contribute prevents unnecessary computations of the objective function. Applying the mutation operator twice, each selected individual generates two offspring. After reproduction, the individual with the intermediate fitness value among a parent and its two offspring is chosen and eliminated because it is less able to identify local optima or local minima, as shown in Fig.3-2.

Individuals not selected for reproduction for many generations are called "non-active" individuals. A threshold parameter $n_a$ is introduced: if an individual is not selected for $n_a$ generations it becomes a non-active individual. Individuals that have an intermediate fitness value in comparison to their neighbours are called "local middle" individuals.

While the algorithm proceeds, the number N of individuals tends to increase, so, at the end of the mutation step, some individuals are eliminated in order to recondition the initial number $N_{pop}$ of individuals in the population

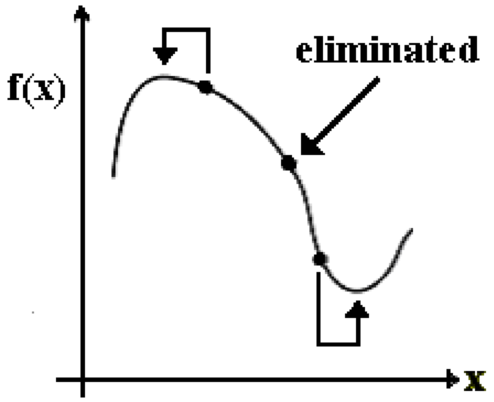

Fig. 3-2 : Elimination of the individual with intermediate fitness value among the parent and the 2 offspring, in a 1-dimensional search space.

Non-active and local-middle individuals are mainly suitable to be eliminated. The pseudo-code of the elimination mechanism is shown in Fig. 3-3.

```
- begin elimination
    - number of exceeding individuals: $N_e = N - N_{pop}$
    - number of non-active individuals: $N_{na}$
    - number of local-middle individuals: $N_{lm}$
    - if $N_e > N_{na}$
        - elimination of all non-active individuals
        - $N_e = N_e - N_{na}$
        - if $N_e > N_{lm}$
            - elimination of all local-middle individuals
            - $N_e = N_e - N_{lm}$
        - else
            - elimination of the $N_e$ worst local-middle individuals
            - $N_e = 0$
        - endif
    - else
        - elimination of the $N_e$ worst non-active individuals
        - $N_e = 0$
    - endif
- end elimination
```

Fig. 3-3. Pseudo-code of the elimination mechanism.

If, for several consecutive times, an individual selected for reproduction generates two offspring with fitness values lower than its own, then we assume that it is probably a maximum and we call it a "hypothetical maximum". A minimum can be identified analogously: we call an individual that generates, several consecutive times, offspring with fitness values higher than its own a "hypothetical minimum" . Two numbers $n_H$ and $n_L$ are fixed in order to quantify the meaning of "several times" for the identification of hypothetical maxima and minima respectively.

Two hypothetical maxima belong to the same niche if their Euclidean distance is lower than both their niche radii. If only one hypothetical maximum has a niche radius $r_1$ greater than their Euclidian distance, this niche radius is reduced:

$$r_{1,new} = r_{1,old} - r_2 \tag{3.8}$$

where $r_2$ is the niche radius of the other hypothetical maximum.

The hypothetical maxima belonging to the same niche and having fitness values lower than that of the best hypothetical maximum in the niche are called "doublets". At the end of the main loop all doublets are deleted.

A deterministic search is then started from each hypothetical maximum and carried out by means of the PS algorithm. At the end of the PS, the niche radii are updated and new doublets are deleted, if they occur. The remaining hypothetical maxima are the optimal solutions obtained and their niche radii provide a measure of the sensitivity of the maxima to variations in the design parameters.

A comparison among the SALHE-EA, Niched Genetic Algorithm (NGA) and Artificial Immune System (AIS) on both newly designed and existing test functions, typically used for NGA benchmarking demonstrated that using the same number of evaluations SALHE-EA works better than both NGA and AIS [52]. Moreover, SALHE-EA approaches the performance of the other algorithms with a smaller number of objective function evaluations, showing that it is well-suited when the containment of computational cost is a priority, as in electromagnetic optimization. SALHE-EA works better than other two algorithm also on functions with unequally spaced and non-uniform peaks.

## 3.3 The Parallel version of SALHE-EA

In the optimization of electromagnetic devices the computation effort due to the steps of the SALHE-EA is negligible compared to the time need to obtain a numerical solution. Moreover in each niche a PS is performed and, of course, they can run in parallel. Furthermore since PS always starts from a point close to the optimum it converges with a little number of objective function evaluations. So, in order to estimate the overall optimization time only the number of objective function evaluations of the SALHE-EA stochastic section is relevant. In particular, each generation two individuals are selected for mutation by means of two different mechanisms. Each selected individual breeds two times.

The fitness of the four generated individuals is computed. Note that in case of parallel computing this behavior makes ineffective the use of more than four CPU. Hence, for the stochastic section, the number of objective function evaluations $nv$ is equal to:

$$nv = 4ng + N \tag{3.9}$$

where $ng$ is the number of generations and N the initial population size. Therefore assuming that fitness evaluation needs an average time $T_s$ for each individual, the overall optimization time $T_{tot}$ is about:

$$T_{tot} = (4ng + N)T_s \tag{3.10}$$

Parallelizing SALHE-EA using a standard master/slave model [54] involves a lower limit on the overall optimization time equal to:

$$T_{tot} = (1 + ng)T_s \approx \frac{nvT_s}{4} \tag{3.11}$$

In fact, a simple parallel version of SALHE-EA, requires (using a number of $N_{CPU} \geq N$) a time $T_s$ for the initial population fitness evaluation plus a time $ngT_s$ for the offspring fitness evaluation. The Parallel SALHE-EA

(PSALHE-EA) presented here has some new features that permit to considerably reduce the overall optimization time respect to the theoretical limit (3.11).

PSALHE-EA and SALHE-EA have the same following characteristics:

- the evaluating method of the modified fitness;
- the niche radius definition and its estimation method;
- the identification method of hypothetical maxima and minima;
- the roulette wheel selection operator is applied; two wheels are created: W1 with slots proportional to $f_H$ (modified fitness used to search for the maxima) and W2 with slots proportional to $f_L$ (modified fitness used to search for the minima);
- the mutation mechanism;
- the elimination mechanism of “doublets”;
- the coupling with the deterministic PS algorithm.

PSALHE-EA differs from SALHE-EA in these aspects:

- the number of individuals selected for reproduction each generation can be chosen by user (2 individuals are selected in SALHE-EA);
- each selected individual generates only one offspring (2 in SALHE-EA);
- the absence in PSALHE-EA of the mechanism of elimination of useless individuals;

- the introduction in PSALHE-EA of a replacement mechanism of the individuals that are identified as hypothetical maxima or minima and stored in an external archive and for this reason deleted from the population; they are replaced by new individuals randomly generated;
- the comparison mechanism applied to the fitness of parents and offspring after reproduction.

In PSALHE-EA, when the parent is selected by means of wheel W1, such mechanism replaces the parent $i$ with the offspring $j$ with the greatest fitness $f_j$ if $f_j>f_i$. In the same way, when the parent is selected by means of wheel W2, the parent $i$ is replaced by the offspring $j$ with the smallest fitness $f_j$ if $f_j<f_i$. In SALHE-EA, the individual with the intermediate fitness value among a parent and its two offspring is chosen and eliminated because it is less able to identify local maxima or local minima, as shown in Fig.3-2.

The most important feature of PSALHE-EA is the possibility to select more than two individuals for reproduction: $h$ individuals are selected for the reproduction by means of wheel W1 and $l$ by means of wheel W2. This is not feasible using the comparison mechanism of SALHE-EA.

Considering a number of generation equal to *ngp,* the number of objective function evaluations *nvp* is equal to:

$$nvp = N + (h + l)ngp + M + m \tag{3.12}$$

with a overall optimization time:

$$Tp_{tot} = [N + (h+l)ngp + M + m]T_s \tag{3.13}$$

where *M and m* are, respectively, the number of hypothetical maxima and hypothetical minima provided by PSALHE-EA.

Making full use of parallelization this time can be reduced to:

$$Tp_{tot} = (1 + ngp + M + m)T_s \approx \frac{nvpT_s}{h+l} \tag{3.14}$$

Hence, using the same number of evaluations, *nvp*=*nv*, the PSALHE-EA computing time gain respect to SALHE-EA is:

$$Tp_{tot} \approx \frac{4}{h+l} T_{tot} \tag{3.15}$$

where the upper limit to the sum ($h$+$l$) is due to the number of available CPUs.

## 3.4 Numerical validation

The evaluation of performance was carried out applying PSALHE-EA to a set of mathematical functions, and to electromagnetic problems.

### 3.4.1 Mathematical functions

The performance of the PSALHE-EA algorithm was evaluated by means of a test of mathematical functions typically used for multimodal algorithm benchmarking [55], as Shekel's Foxholes function (Fig. 3-4)

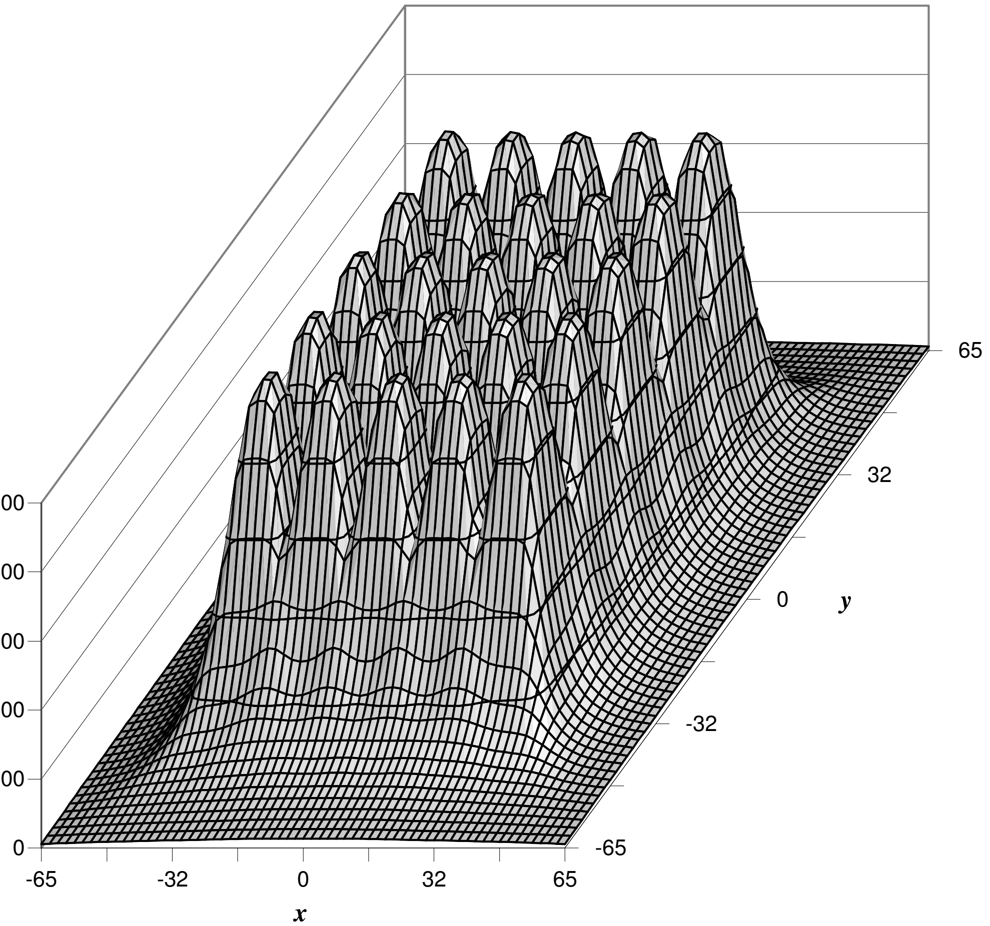

Fig. 3-4. Shekel's foxholes function

The chosen values for algorithm parameters were $a_H$=$b$=$c$=1, $e$=1. Three different values for population size were used: $N$=10 ($n_c$=3, $nh$=5, $nl$=4), $N$=20 ($n_c$=4, $nh$=6, $nl$=5), $N$=25 ($n_c$=5, $nh$=8, $nl$=6). The results on mathematical functions are averaged over 100 trials.

Table I and Table II show the percentage of authentic maxima found on Shekel's Foxholes function (over 25 true maxima). Table 3-I shows results obtained on a single CPU, i.e. without parallelization. The new strategy adopted in PSALHE-EA gives comparable results using the same number of offspring of SALHE-EA ($h$ = $l$ = 2) and about the same overall optimization time. Table 3-II shows results for the case of $h$=$l$=5: parallel computing drastically reduces the optimization time when $h$ and $l$ increase. The performance decreases only using a very low evaluations number: this  is negligible in case of parallel computing which typically allows a high evaluation number. Fig. 3-5 shows the final hypothetical maxima with their radii in a solution found by means of the SALHE algorithm for the Foxholes function.

TABLE 3-I

COMPARISON BETWEEN SALHE-EA AND PSALHE-EA ON SHEKEL'S FOXHOLES FUNCTION

| $T_{TOT}$ | Ng | Nv | PERCENTAGE OF SUCCESS | |
|---|---|---|---|---|
| | | | SALHE-EA | PSALHE-EA |
| $1000T_s$ | 249 | 1000 | 47.51% | 43.08 % |
| $2500T_s$ | 622 | 2500 | 82.42% | 82.72 % |
| $5000T_s$ | 1173 | 5000 | 92.61% | 94.56 % |

TABLE 3-II

PERFORMANCE OF PSALHE-EA USING PARALLELIZATION

| $T_{tot}$ | *ngp* | *nvp* | PERCENTAGE OF SUCCESS |
|---|---|---|---|
| $\sim 100T_s$ | 91 | 1000 | 33.84 % |
| $\sim 250T_s$ | 229 | 2500 | 77.32 % |
| $\sim 500T_s$ | 472 | 5000 | 94.20 % |

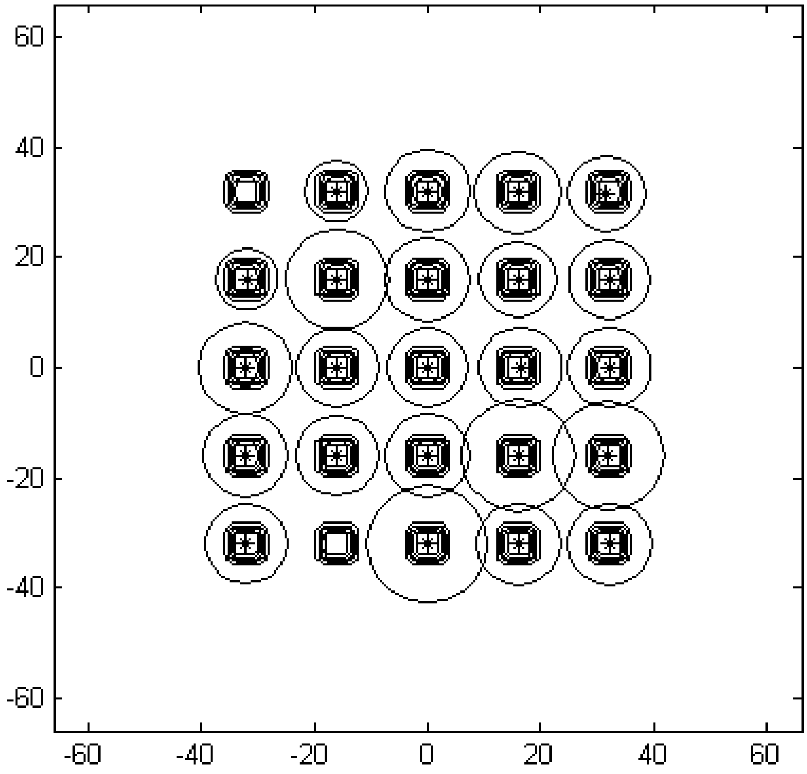

Fig. 3-5: Final hypothetical maxima with their radii for the Foxholes function

The validation was also performed by means of an electromagnetic problem: the TEAM Workshop Problem 22 (SMES) [56].

The problem consists of two concetric coils carrying current with opposite direction (Fig. 3-6). Working under superconducting conditions offers the opportunity to store a significant amount of energy in magnetic fields while keeping the stray field with certain limits. An optimal design of the system should couple the desired value of energy $E=E_{ref}$ to be stored (first objective) with a minimal stray field measured at the distance of 10 meters from the device (second objective). Moreover the superconductivity must be guaranteed (quench condition).

An optimization problem with three parameters (radius $R_2$, height $h_2$ and thickness $d_2$ of the outer coil) was defined. Table 3-III shows the variation range of the design parameters.

TABLE 3-III

Design parameters for the SMES problem

| | $R_1$ [m] | $R_2$ [m] | $h_1/2$ [m] | $h_2/2$ [m] | $d_1$ [m] | $d_2$ [m] | $J_1$ [A/mm$^2$] | $J_2$ [A/mm$^2$] |
|---|---|---|---|---|---|---|---|---|
| min | | 2.6 | - | 0.204 | - | 0.1 | | - |
| max | | 3.4 | - | 1.1 | - | 0.4 | | - |
| fixed | 2.0 | - | 0.8 | - | 0.27 | - | 22.5 | -22.5 |

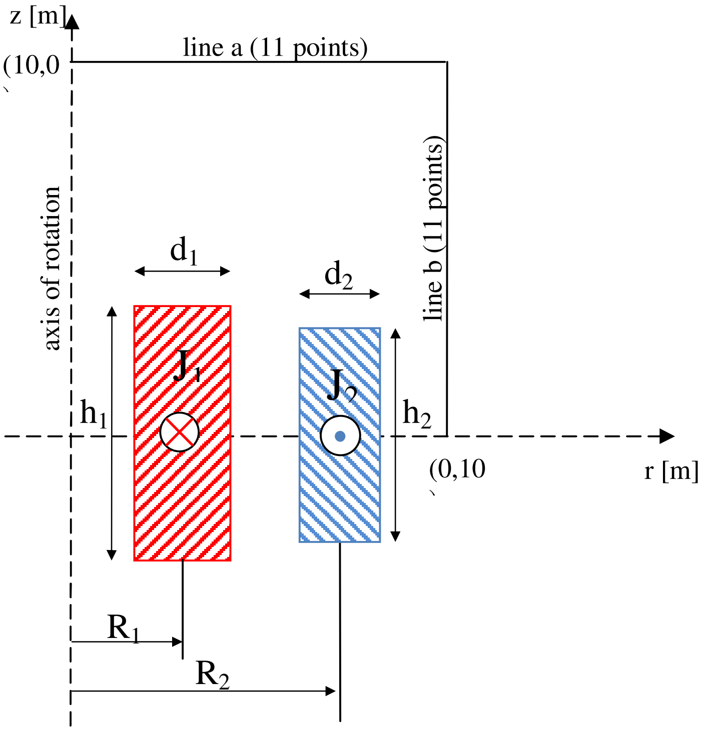

Fig. 3-6: SMES configuration

The objective function of this problem has to take both the energy requirement (E should be as close as possible to 180 MJ) and the stray field requirements ($B_{stray}$ evaluated along 22 equidistant points along line a and line b in Fig. 3-6 as small as possible) into account, hence the problem is a multiobjective problem. However, the two objectives are mapped into a single objective function OF:

$$OF=\frac{B_{stray}^2}{B_{norm}^2}+\frac{\left|E-E_{ref}\right|}{E_{ref}} \tag{3.16}$$

where $E_{ref}$=180 MJ, $B_{norm}$ =200 μT and $B^2_{stray}$ is defined as:

$$B^2_{stray} = \frac{\sum_{i=1}^{22} \left| B_{stray_i} \right|^2}{22} \tag{3.17}$$

The superconducting material should not violate the quench condition that links together the value of the current density and the maximum value of magnetic flux density, as shown in Fig 3-7.

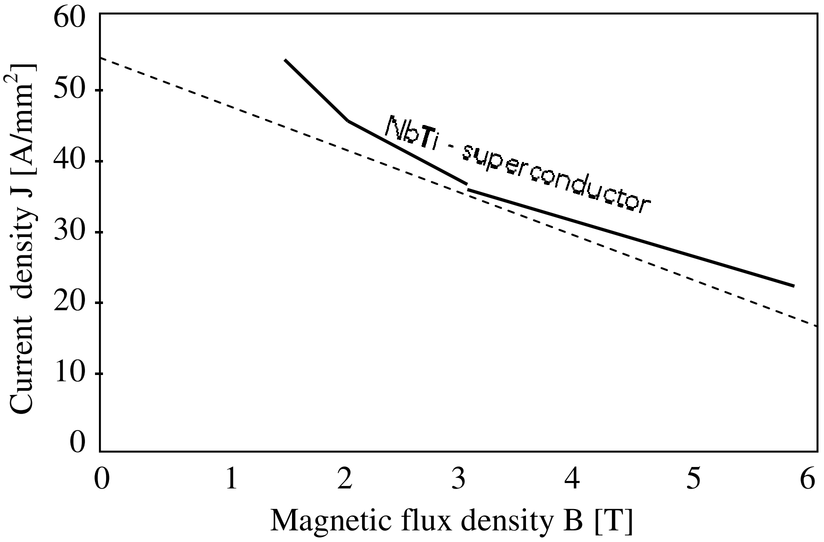

Fig. 3-7: Critical curve of an industrial superconductor.

The critical curve has been approximated by:

$$|J| = (-6.4|B| + 54.0)\, A/mm^2 \tag{3.18}$$

The optimization required 1186 objective function evaluations and a computational time of about 120$T_s$ (100$T_s$ for PSALHE-EA, 20$T_s$ for PS). The method identified four niches: Table 3-IV ($h$ = $l$ = 5) shows values of each optimum, together with the estimated normalized niche radius ρ. The optima and the niche radii are comparable with known solutions [46], [56]. Fig. 3-8 shows the contours of the magnitude of magnetic vector potential A for the optimum O1.

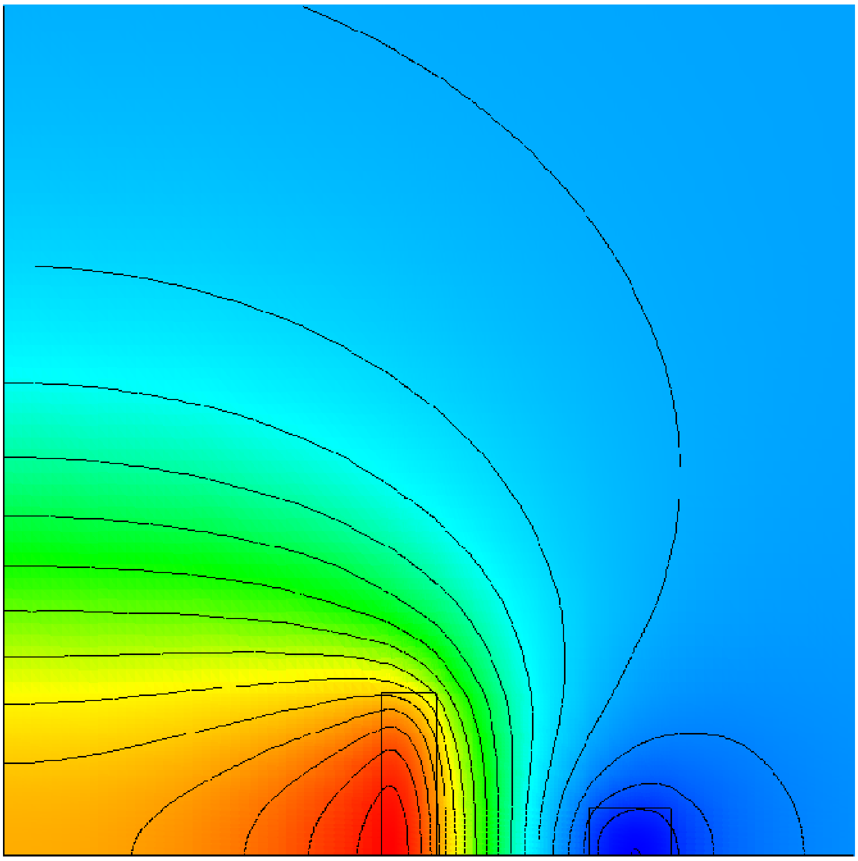

Figura 3-8: Contours of the magnitude of magnetic vector potential A for the optimum O1

TABLE 3-IV

OPTIMA FOR THE SMES BENCHMARK

| | $R_2$ | $h_2/2$ | $d_2$ | OF | ρ |
|---|---|---|---|---|---|
| O1 | 3.0949 | 0.2543 | 0.3658 | 0.08944 | 0.0814 |
| O2 | 3.1771 | 0.3903 | 0.2274 | 0.10143 | 0.0856 |
| O3 | 3.3422 | 0.7815 | 0.1025 | 0.14520 | 0.2284 |
| O4 | 3.1189 | 0.3115 | 0.2949 | 0.09261 | 0.0723 |

## 3.5 Optimization of an induction heating device

The considered electromagnetic device is a induction heater for conductor pieces [57]. The piece is a parallelepiped of aluminum, whose dimensions are L × L × H (L=80mm, H=200mm). The piece is surrounded by a concentric circular inductor of rectangular cross section with thickness s=20mm, which carries a current with constant current density J=4A/mm$^2$ (see Fig. 2).

The design parameters of the inductor are the internal radius r ∈ [60, 80] mm, the height a ∈ [100, 140] mm, the offset between the center of the piece and the center of the inductor in z direction c ∈ [0, 20] mm, the current frequency f ∈ [250, 3000] Hz.

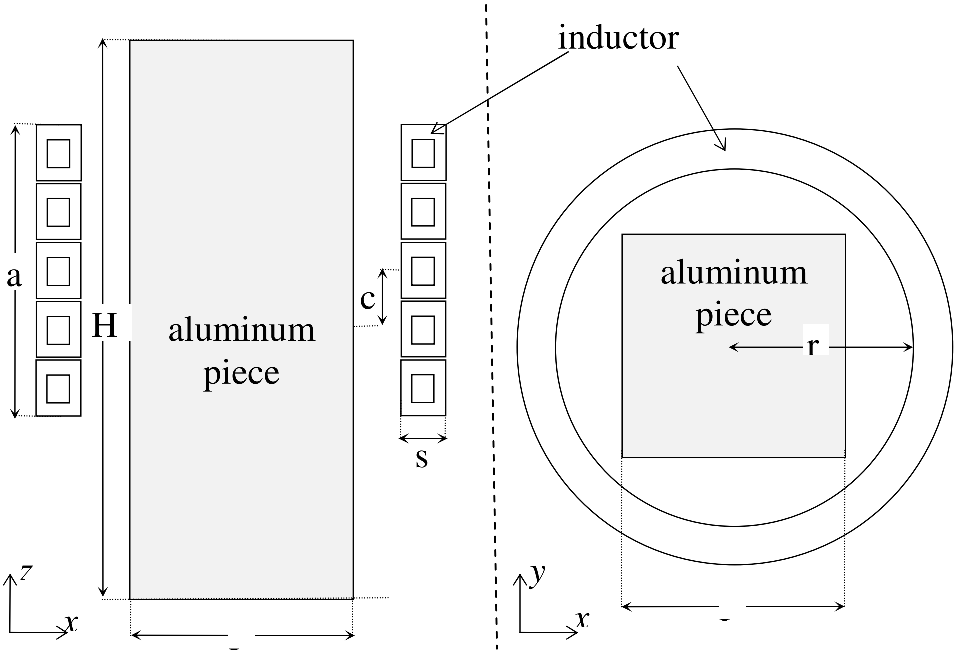

Fig. 3-9: Geometry of the induction heating device

The aim of optimization is to obtain, at the end of the heating, the following three targets:

- minimizing the difference $T_{diff}$ between the steady state average temperature in the piece $T_{av}$ and the desired temperature $T_{ref}$=500°C;
- minimizing the gap of temperature $T_{gap}$ into the piece;
- maximize the induction efficiency η, defined as follows:

$$\eta = P_l/(P_l + P_{ind}) \tag{3.19}$$

where $P_l$, $P_{ind}$ represent the power dissipation in the aluminum piece and in the inductor, respectively.

A compromise between the three objectives is obtained by using fuzzy techniques, which furthermore allow the handling of design objectives which are measured on different scales [58]. Three sigmoidal membership functions were used to scale values in the range [0,1]. The two limits ($y_{acc}$ and $y_{rej}$, respectively the acceptability and unacceptability threshold for each objective) are set according to the designer's requirements. The three membership functions are plotted in Fig. 3-10.

The global objective function OF to maximize is

$$OF = (\mu_{diff} + \mu_{gap} + \mu_{\eta})/3 \tag{3.20}$$

$\mu_{diff}$, $\mu_{gap}$ and $\mu_{\eta}$ being the fuzzified values of the objectives.

Note that both aluminum thermal conductivity and electric conductivity are functions of the temperature, so that the electromagnetic-thermal coupled problem is non linear.

The mesh was refined by means of the mesh generator of Par. 1.6. The initial coarse mesh consists of 525 nodes, 1600 tetrahedra and 2476 edges. Starting from this solution the error indicators $\eta_i$ and the relative probabilities $\pi_i$ are computed. The artificial neural network mesh generator was applied with a target value of additional nodes $N_{add}$=600. The final mesh, which is constituted by 1125 nodes, 4357 tetrahedra and 6230 edges, remained the same during the whole optimization. Fig. 3-11 shows the two meshes.

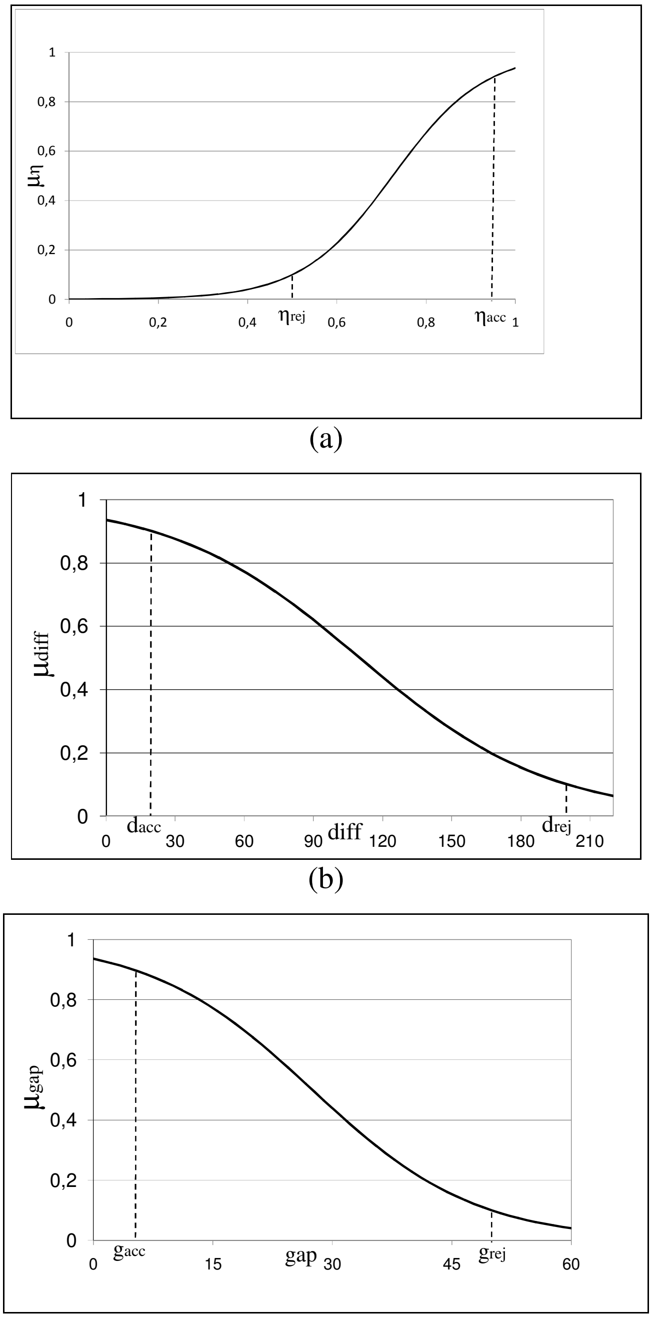

(a)

(b)

(c)

Fig. 3-10: membership functions for the three objectives

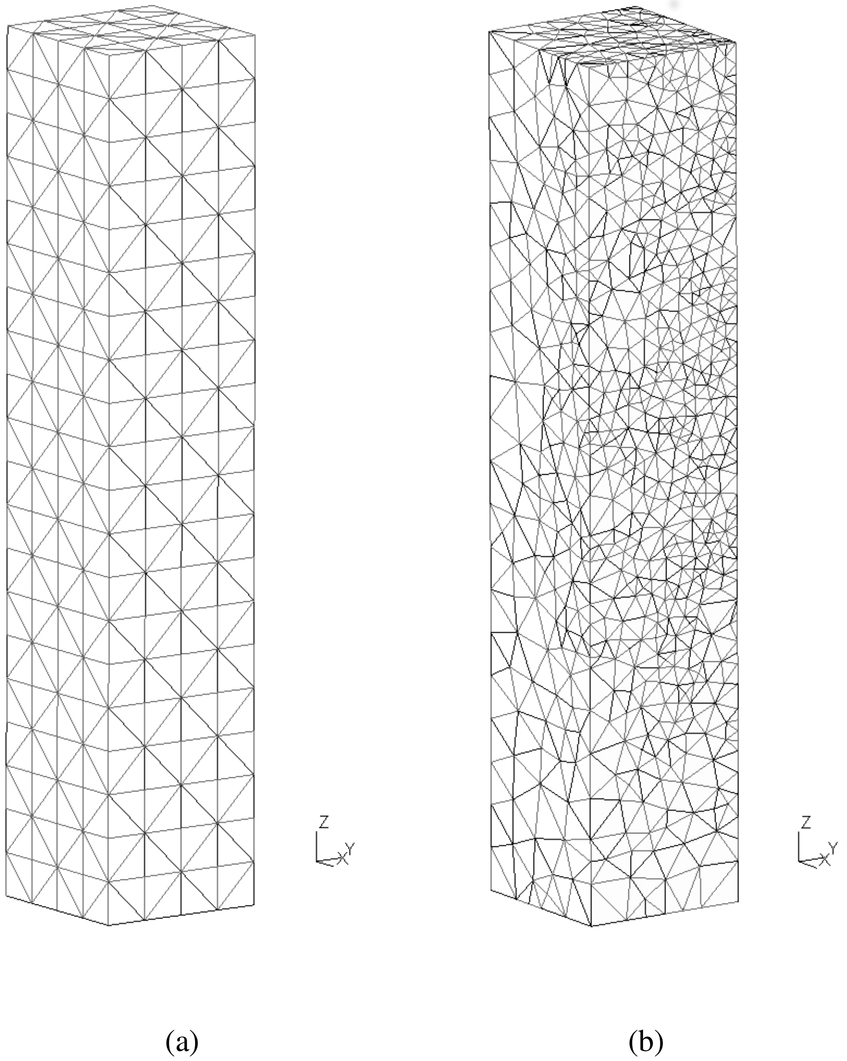

(a) (b)

Fig. 3-11: Initial (a) and final (b) mesh

The thermal analysis was performed employing the strategy explained in chapter 2. Homogeneous Neumann conditions were imposed on the xz and yz planes. The simulation was performed on a computing cluster of 10 PC (P4 3.2

GHz, 4Gb RAM). The total time $T_s$ for the solution of the coupled problem is about 50s. The PSALHE-EA was applied using a initial population N=20, with parameters value h=l=5. The optimization required 2717 OF evaluations and a computational time of about 275 $T_s$ (250$T_s$ for stochastic section of PSALHE-EA, 25$T_s$ for PS).

The CPU time increases of about 875% solving the same problem by means of SALHE-EA. Table 3-V shows the optima values and estimated niche radii ρ of each niche. Fig. 3-12 shows the power density distribution and the temperature distribution for the optimum O3.

TABLE 3-V
OPTIMA FOR THE INDUCTION HEATING DEVICE OPTIMIZATION

| | r<br>[mm] | c<br>[mm] | a<br>[mm] | f<br>[Hz] | OF | ρ | $T_{av}$<br>[°C] | $T_{gap}$<br>[°C] | η<br>[%] |
|---|---|---|---|---|---|---|---|---|---|
| O1 | 77.21 | 10.54 | 101.3 | 1217 | 0.814 | 0.178 | 499.8 | 18.2 | 86.3 |
| O2 | 65.16 | 14.74 | 137.9 | 382 | 0.828 | 0.186 | 499.9 | 14.1 | 84.4 |
| O3 | 67.92 | 13.55 | 127.5 | 487 | 0.824 | 0.196 | 499.9 | 15.4 | 84.9 |

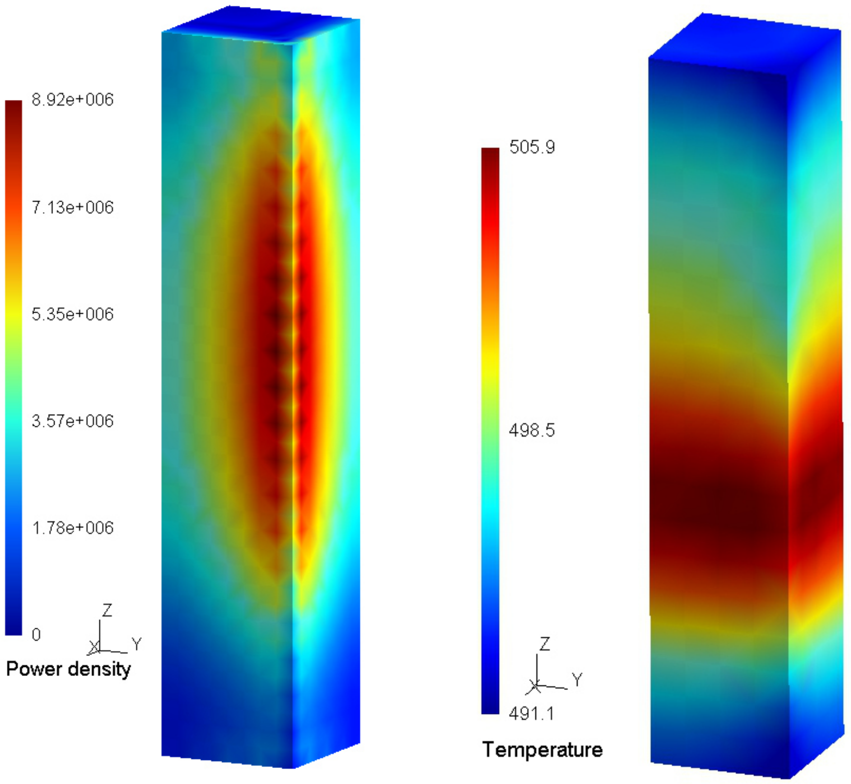

Fig. 3-12: power density and temperature distribution for the optimum O3

# CONCLUSION

In this work an innovative approach to the analysis and synthesis of three dimensional induction heating devices has been proposed.

Analyses and evaluations are performed by means of a hybrid method called FEM-SDBCI (Singular Dirichlet Boundary Condition Iteration). The method couples a differential equation for the interior problem in terms of the electric fields with an integral equation for the exterior one. The adoption of a single vector unknown in both the conductors and the air does not involve a significant increase in computational cost as compared with other Eddy Current formulations. The method alleviates the major drawback of FEM-DBCI, that is, the insertion of some element layers between the integration and truncation surfaces; consequently, the integral equation becomes singular. The method is similar to the well-known FEM-BEM, but it assumes a Dirichlet boundary condition on the truncation boundary instead of a Neumann one. FEM-SDBCI leads to shorter solving times with respect to FEM-BEM. The FEM-SDBCI allows, in coupled problems, the use of a unique finite element mesh for both electromagnetic and thermal analyses.

The FEM-SDBCI is then incorporated in a method for the computation of the heating of a conductor in which eddy currents flow, induced by time-harmonic source currents. The electrical field is assumed to be unknown on a mesh of edge elements and is computed by a time-harmonic analysis which uses the hybrid FEM-DBCI method. The heating power density inside the conductor is computed and a transient thermal analysis is started on the same mesh of nodal elements. This analysis is continued until the temperature-dependent electrical conductivity or the magnetic reluctivity changes enough to require another time-harmonic eddy-current analysis. This combined procedure is iterated. To solve the transient non linear problem, a Crank-Nicolson scheme was implemented.

Moreover, FEM-SDBCI is particularly suitable for use in an optimization tool. In fact, in the case of design of induction heating device, it allows a great saving of computing time by treating current sources as external sources, avoiding the construction of an FEM matrix in each solution of the field problem and making use of the same mesh for both electromagnetic and thermal problem. The optimization algorithm presented in this work is the PSALHE-EA algorithm for optimization of electromagnetic devices. The PSALHE-EA has some new features that permit to reduce considerably the overall optimization time allowing to make full use of parallelization. The tests performed show that PSALHE-EA is a very efficient hybrid optimization method, that always outperforms the serial version. The ability to find multiple optima with a low computing time makes the algorithm particularly suitable to be used in the design of electromagnetic devices. Finally an induction heating system has been designed in order to validate the method with an industrial application, obtaining several good solutions at low computational costs

# Appendix A

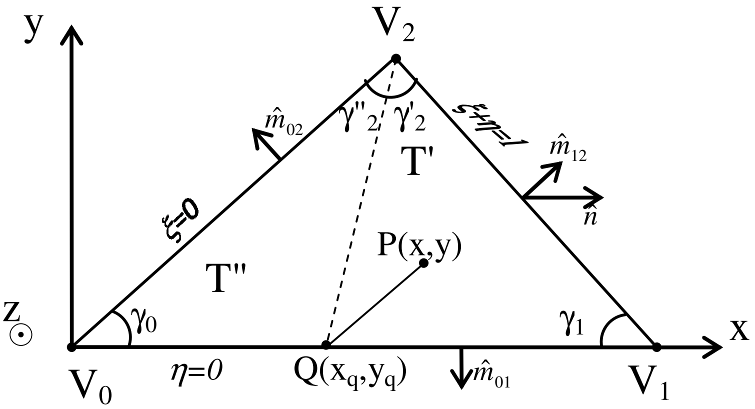

Fig A-1. Triangular patch

Let consider a generic triangular patch $T_k$. A local coordinate frame is selected, in such a way that $T_k$ lies on the xy plane, vertex $V_0$ coincides with the origin and the other two vertices have coordinates $V_1=(x_1,0,0)$ and $V_2=(x_2,y_2,0)$.The integral

$$I = \iint_{T_k} (ax + by + c) \frac{\partial}{\partial x} \frac{1}{r} dxdy \tag{A.3}$$

where *a*, *b* and *c* are given coefficients; in the triangular domain $T_k$ can be conveniently performed by subdividing the patch in two subtriangles T' and T'' (fig. A-1).

In T$_k$, a system of coordinates (ξ,η) can be related to the system (x,y) as follows:

$$\begin{cases} x = x_1\xi + x_2\eta \\ y = y_2\eta \end{cases} \tag{A.2}$$

Let split the integral in (A.1):

$$I = \iint_{T_k} (ax+by+c)\frac{\partial}{\partial x}\frac{1}{r}dxdy = \iint_{T_k} (ax+by)\frac{\partial}{\partial x}\frac{1}{r}dxdy + \iint_{T_k} c\frac{\partial}{\partial x}\frac{1}{r}dxdy \tag{A.3}$$

The first integral in the right and side of (A.3) can be calculated as follows:

$$I_{ab} = \iint_{T_k} (ax+by)\frac{\partial}{\partial x}\frac{1}{r}dxdy = \iint_{T_k}\left(\frac{ax+by}{r}\right)dxdy - a\iint_{T_k}\frac{1}{r}dxdy = \iint_{T_k}\left(\frac{ax+by}{r}\right)dxdy - aI_o \tag{A.4}$$

The terms I$_0$ is computed as in (1.41). Thanks to the Green theorem (A.4) leads to:

$$I_{ab} = \oint_{\partial T_k} \frac{ax+by}{r}\hat{m}\cdot\hat{n}\,dl - aI_0 \tag{A.5}$$

being $\hat{m}$ the unit normal vector directed outside to $\partial T_k$. Considering that

$$\hat{m}_{12}\cdot\hat{n} = \cos(\pi/2 - \gamma_1) = sen\gamma_1 \tag{A.6}$$

$$\hat{m}_{20}\cdot\hat{n} = \cos(\pi/2 + \gamma_0) = -sen\gamma_0 \tag{A.7}$$

$$\hat{m}_{01}\cdot\hat{n} = 0 \tag{A.8}$$

and by means of (a.2), eq. (a.5) changes as :

$$
\begin{aligned}
I_{ab} &= sen\gamma_1 \int_0^1 \frac{a[x_1(1-\eta)+x_2\eta]+by_2\eta}{\sqrt{(x_1+(x_2-x_1)\eta-x_q)^2+(y_2\eta)^2}}d\eta\ + \\
&\quad - sen\gamma_0 \int_0^1 \frac{ax_2\eta+by_2\eta}{\sqrt{(x_2\eta-x_q)^2+(y_2\eta)^2}}d\eta\ -aI_0
\end{aligned}
\tag{A.9}
$$

Using the notation:

$$R=A+B\eta+C\eta^2 \tag{A.10}$$

integrals in (A.9) are of the form which can be evaluated by means of the following analytical formulas [23]:

$$\int \frac{\eta d\eta}{\sqrt{R}} = \frac{\sqrt{R}}{C} - \frac{B}{2C}\int \frac{d\eta}{\sqrt{R}} \tag{A.11}$$

$$\int \frac{d\eta}{\sqrt{R}} = \frac{1}{\sqrt{C}}\ln\left(2\sqrt{C\,R}+2C\eta+B\right) \tag{A.12}$$

Defining $R_1(\eta)=A_1+B_1\eta+C_1\eta^2$ and $R_2(\eta)=A_2+B_2\eta+C_2\eta^2$, with $A_1=(x_1-x_q)^2$, $A_2=x_q^2$, $B_1=2(x_1-x_q)\ (x_2-x_1)$, $B_2=-2x_qx_2$, $C_1=(x_2-x_1)^2+y_2^2$, $C_2=x_2^2+y_2^2$, by means of (A.11) and (A.12), equation (A.9) leads to:

$$
\begin{aligned}
I_{ab} &= sen\gamma_1 L_{12}\left\{ax_1\left[F_1^{'}(\eta)\right]_0^1+(a(x_2-x_1)+by_2)\left[\left[\frac{\sqrt{R_1}}{(x_2-x_1)^2+y_2^2}-\frac{(x_2-x_1)(x_1-x_q)}{\left((x_2-x_1)^2+y_2^2\right)}\cdot F'(\eta)\right]_0^1\right\}+ \\
&\quad - sen\gamma_0 L_{02}(ax_2+by_2)\left[\frac{\sqrt{R_2}}{x_2^2+y_2^2}+\frac{x_2x_q}{x_2^2+y_2^2}F''(\eta)\right]_0^1 - aI_0
\end{aligned}
\tag{A.13}
$$

where $L_{12}$ and $L_{02}$ are the lengths of two edges of the triangles, and

$$F^{'}(\eta)=\frac{1}{\sqrt{(x_2-x_1)^2+y_2^2}}\cdot$$
$$\ln\left(2\sqrt{(x_2-x_1)^2+y_2^2}\sqrt{R_1}+2\left[(x_2-x_1)^2+y_2^2\right]\eta+2(\mathrm{x}_1-\mathrm{x}_\mathrm{q})(\mathrm{x}_2-\mathrm{x}_1)\right) \tag{A.14}$$

$$F^{''}(\eta)=\frac{1}{\sqrt{{x_2}^2+y_2^2}}\cdot\ln\left(2\sqrt{{x_2}^2+y_2^2}\sqrt{R_2}+2\left[{x_2}^2+y_2^2\right]\eta-2\mathrm{x}_\mathrm{q}\mathrm{x}_2\right) \tag{A.15}$$

then, evaluating (A.13) at integration's extremes:

$$I_{ab}=sen\gamma_1L_{12}\left\{ax_1G^{'}+(a(x_2-x_1)+by_2)\left[\frac{\overline{V_2Q}-\overline{V_1Q}}{(x_2-x_1)^2+y_2^2}-\frac{(x_2-x_1)(x_1-x_q)}{\left((x_2-x_1)^2+y_2^2\right)}\cdot G^{'}\right\}+$$
$$-sen\gamma_0L_{02}(ax_2+by_2)\left[\frac{\sqrt{R_2}}{{x_2}^2+y_2^2}+\frac{x_2x_q}{{x_2}^2+y_2^2}G''\right]-aI_0 \tag{A.16}$$

where:

$$G'=\frac{1}{\sqrt{(x_2-x_1)^2+y_2^2}}\ln\frac{\sqrt{(x_2-x_1)^2+y_2^2}\,\overline{V_2Q}+\overline{V_1V_2}^2+(\mathrm{x}_1-\mathrm{x}_\mathrm{q})(\mathrm{x}_2-\mathrm{x}_1)}{\sqrt{(x_2-x_1)^2+y_2^2}\,\overline{V_1Q}+(\mathrm{x}_1-\mathrm{x}_\mathrm{q})(\mathrm{x}_2-\mathrm{x}_1)} \tag{A.17}$$

$$G''=\frac{1}{\sqrt{{x_2}^2+y_2^2}}\ln\frac{\sqrt{{x_2}^2+y_2^2}\,\overline{V_2Q}+\overline{V_2V_0}^2-\mathrm{x}_\mathrm{q}\mathrm{x}_2}{\sqrt{{x_2}^2+y_2^2}\,\overline{V_0Q}-\mathrm{x}_\mathrm{q}\mathrm{x}_2} \tag{A.18}$$

Finally the following equation can be obtained:

$$I_{ab}=\frac{sen\gamma_1L_{12}}{\overline{V_1V_2}^2}\left\{ax_1H'+(a(x_2-x_1)+by_2)\left[\overline{V_2Q}-\overline{V_1Q}+\overline{V_1Q}\cdot\cos\gamma_1\cdot H'\right\}+$$
$$-\frac{sen\gamma_0L_{02}}{\overline{V_2V_0}^2}(ax_2+by_2)\left[\left[\overline{V_2Q}-\overline{V_0Q}+\overline{V_0Q}\cdot\cos\gamma_0\cdot H''\right]-aI_0 \tag{A.19}$$

where:

$$H' = \ln \frac{\overline{V_2Q} + \overline{V_1V_2} - \overline{V_1Q}\cos\gamma_1}{\overline{V_1Q}(1-\cos\gamma_1)} \tag{A.20}$$

$$H'' = \ln \frac{\overline{V_2Q} + \overline{V_2V_0} - \overline{V_0Q}\cos\gamma_0}{\overline{V_0Q}(1-\cos\gamma_0)} \tag{A.21}$$

In a similar way the second integral in the right and side of (A.3) can be calculated as follows,:

$$I_c = \iint_{T_k} c\frac{\partial}{\partial x}\frac{1}{r}\,dxdy = \oint_{\partial T_k} \frac{c}{r}\,\hat{m}\cdot\hat{n}\,dl \tag{A.22}$$

The right and side of (A.22) has the same form of (A.12) and, making use of an approach analogous to (A.12)-(A.21), leads to:

$$I_C = c\frac{sen\gamma_1 L_{12}}{\overline{V_1V_2}}H' - c\frac{sen\gamma_0 L_{02}}{\overline{V_2V_0}}H'' \tag{A.23}$$

where H' and H" are the same of (A.20)-(A.21). If Q is a generic Gauss points $P_n=(\xi_n x_1,0,0)$ $(0<\xi_n<1)$ in the triangle, the equations (A.19) and (A.23), applying substitutions (1.44)-(1.51), lead to equation (1.43).

# REFERENCES

[1] P. P. Silvester, R. L. Ferrari, "*Finite Elements for Electrical Engineers*", $3^a$ ed., Cambridge University Press, Cambridge, 1996.

[2] O. Biro, K. Preis, "On the use of the Magnetic Vector potential in the Finite Element Analysis of Three-Dimensional Eddy Currents", *IEEE Transaction on Magnetics*, vol. 25, no.4, pp. 3145-3158 , July 1989

[3] A. Krawczyk, J. A. Tegopoulos, "*Numerical Modelling of Eddy currents"*, Oxford University Press, Oxford, 1993.

[4] Z. Ren, A. Razek, "Comparison of Some 3D Eddy Current Formulations in Dual Systems", *IEEE Transaction on Magnetics*, vol. 36, pp. 751-755, July 2000.

[5] E. Dilettoso "Analysis and Optimized Design of Eddy Current Devices", Ph.D. Thesis, Catania (Italy), 2003.

[6] Z. Ren, F. Bouillault, A. Razek, A. Bossavit, J. C. Vérité, "A new hybrid model using electric field formulation for 3-D eddy current problems," *IEEE Transaction on Magnetics*, vol. 26, pp. 470-473, March. 1990.

[7] A. Bossavit, "A rationale for edge-elements in 3-D fields computations," *IEEE Transaction on Magnetics*, vol. 24, pp. 74-79, Jan. 1988.

[8] T. Nakata, N. Takahashi, K. Fujiwara and Y. Okada, "Improvements pf the T-Ω method for 3-D eddy current analysis," *IEEE Transaction on Magnetics*, vol. 24, no. 1, 1988, pp. 94-97.

[9] J. P. Webb and B. Forghani, "A single scalar potential method for 3D magnetostatic using edge elements," *IEEE Transaction on Magnetics*, vol. 25, pp. 4126-4128, 1989.

[10] C. A. Brebbia, J. C. F. Telles, L. C. Wrobel, Boundary Element Technique, Springer-Verlag, Berlin, 1984.

[11] G. Aiello, S. Alfonzetti, and S. Coco, "Charge iteration: a procedure for the finite-element computation of unbounded electrical fields," *Int. J. Numer. Methods Engng*, vol. 37, pp. 4147-4166, December 1994.

[12] G. Aiello, S. Alfonzetti, S. Coco, and N. Salerno, "Finite element iterative solution of skin effect problems in open boundaries," *Int. J. Numer. Modelling*, vol. 9, pp. 125-143, January-April 1996.

[13] G. Aiello, S. Alfonzetti, "Finite element computation of axisymmetric eddy currents in an infinite domain," *Compel*, vol. 19, n. 2, pp. 167-172, 2000.

[14] J. A. Stratton, "*Electromagnetic Theory*," McGraw-Hill, New York, 1941.

[15] S. Alfonzetti, G. Borzì, “Finite Element Solution to Electromagnetic Scattering problems by means of the Robin Boundary Condition Iteration method”, *IEEE Transactions on Antennas and Propagations*, Vol. 50 Issue 2, pp. 132-140, Feb. 2002.

[16] G. Aiello, S. Alfonzetti, E. Dilettoso, "Finite element solution of eddy current problems in unbounded domains by means of the hybrid FEM–DBCI method" IEEE Tans. Magn., vol.39, p.1409-12, May 2003.

[17] L. Greengard, "*The Rapid Evaluation of Potential Fields in Particle* Systems," MIT Press, Cambridge, 1988.

[18] S. J. Salon, and J. D'Angelo, "Applications of the hybrid finite element - boundary element method in electromagnetics," IEEE Trans. Magn., vol. 24, p. 80-85, Jan. 1988.

[19] G. Aiello, S. Alfonzetti, G. Borzì, and N. Salerno, "An improved solution scheme for open-boundary skin effect problems," *IEEE Trans. Magn.*, vol. 37, pp. 3474-3477, Sept. 2001.

[20] G. Aiello, S. Alfonzetti, G. Borzì, E. Dilettoso, N. Salerno, "Efficient solution of skin-effect problems by means of the GMRES-accelerated FEM-BEM method," IEEE Trans.Magn.,vol. 44, p. 1274-77, June 2008.

[21] G. Aiello, S. Alfonzetti, G. Borzì, E. Dilettoso, N. Salerno, "Comparing FEM-BEM and FEM-DBCI for open-boundary electrostatic problems", Europ. Phys. J. – Applied Phys., vol. 39, p 143-148, Aug. 2007.

[22] R.D. Graglia, "On the numerical integration of the linear shape functions times the 3-D Green's function or its gradient on a plane triangle," IEEE Transactions on Antennas and Propagation, vol. 41, p. 1448-1455, 1993.

[23] D. Zwillinger, "Table of Integrals, Series, and Products", Academic Press, 2007.

[24] G. Aiello, S. Alfonzetti, G. Borzì, E. Dilettoso, "Solution of Open-Boundary Eddy Current Problems by means of the FEM-SDBCI Method", Biennial IEEE Conference on Electromagnetic Field Computation, Oita (J), November 11-14, 2012. Engineering, Zurich (CH), September 11-14, 2012.

[25] G. Aiello, S. Alfonzetti, E. Dilettoso, "Eddy Current Calculation by means of the Singular FEM-DBCI Method", International Symposium on Electromagnetic Fields in Electrical Engineering, Madeira (P), September 1-3, 2011.

[26] L. A. Hageman and D. M. Young, *Applied Iterative Methods*, Academic Press, S. Diego, 1981.

[27] Y. Saad and M. H. Schultz, "GMRES: a generalized minimal residual algorithm for solving nonsymmetric linear systems," *SIAM J. Sci. Stat. Comput.*, vol. 7, n. 3, pp. 856-869, July 1986.

[28] G. Aiello, S. Alfonzetti, G. Borzì, N. Salerno, "An improved solution scheme for open-boundary skin effect problems," *IEEE Transaction on Magnetics*, vol. 37, n. 5, pp. 3474-3477, Sept. 2001.

[29] G. Aiello, S. Alfonzetti, G. Borzì, E. Dilettoso, N. Salerno, "GMRES Solution of FEM-BEM Global Systems for Electrostatic Problems without Voltaged Conductors", IEEE Transactions on Magnetics, vol. 49, n. 5, 2013, pp. 1701-1704.

[30] G. Aiello, S. Alfonzetti, G. Borzì, E. Dilettoso, N. Salerno, "A Modified FEM-DBCI Method for Static and Quasi-Static Electromagnetic Field Problems", IEEE Transactions on Magnetics, vol. 46, n. 8, august, 2010, pp. 2803-2806.

[31] Z. J. Cendes and D. N. Shenton, "Adaptive mesh refinement in the finite element computation of magnetic fields," *IEEE Transactions on Magnetics*, vol. 21, pp. 1811-1816, September 1985.

[32] N. A. Golias and T. D. Tsiboukis, "An approach to refining three-dimensional tetrahedral meshes based on Delaunay transformations," *Int. J. Numer. Meth. Eng.,* vol. 37, pp. 793-812, 1994.

[33] S. Alfonzetti, S. Cavalieri, S. Coco, M. Malgeri, "Automatic mesh generation by the Let-It-Grow neural network," *IEEE Transactions on Magnetics*, vol. 32, pp. 1349-1352, May 1996.

[34] S. Alfonzetti, "High-quality mesh generation by an artificial neural network," *IGTE Symposium,* Graz (Austria), September 23-25, 1996.

[35] S. Alfonzetti, "A finite element mesh generator based on an adaptive neural network," *IEEE Transactions on Magnetics,* vol. 34, no. 5, pp. 3363-3366, September 1998.

[36] S. Alfonzetti, "A Neural Network Generator for Tetrahedral Meshes," *IEEE Transactions on Magnetics,* vol. 39, no.3, pp. 1650-1653, May 2003.

[37] S. Alfonzetti, E. Dilettoso, N. Salerno, "An optimized generator of finite element neshes based on a neural network", *IEEE Transactions on Magnetics*, vol. 44, no. 6, pp. 1278-1281, June 2008.

[38] S. Alfonzetti, E. Dilettoso, N. Salerno, "A Neural Network Mesh Generator for Eddy Current Problems", *International Symposium on Electromagnetic Fields in Electrical Engineering*, Ohrid (MK), September 12-14, 2013.

[39] G. Aiello, S. Alfonzetti, G. Borzì, N. Salerno, "An overview of the ELFIN code for finite element research in electrical engineering", *Electrosoft'99*, Seville (E), May 17-19 May, 1999.

[40] G. Aiello, S. Alfonzetti, E. Dilettoso, N. Salerno, "A Software Tool for Stochastic Optimization of Electromagnetic Devices", *Software for Electrical Engineering Analysis and Design V, Wessex Institute of Technology Press*, 2001, pp. 175-184.

[41] L. R. Turner et alii, "Problems and workshops for eddy current code comparison," *IEEE Transaction on Magnetics*, vol. 24, pp. 431-434, Jan. 1988.

[42] D. Zheng, "Three-dimensional eddy current analysis by the boundary element method", *IEEE Transactions on Magnetics,* Vol. 33 n°2, pp. 1354-1357, March 1997.

[43] T. J. R. Hughes, "Unconditionally stable algorithms for nonlinear heat conduction", *Computer Methods in Applied Mechanics and Engineering*, vol. 10, pp. 135-139, 1977

[44] G. Aiello, S. Alfonzetti, E. Dilettoso, N. Salerno, "Transient Thermal Analysis of an Eddy-Current Heated Conductor Applying FEM-DBCI", *IEEE Transactions on Magnetics*, vol. 49, n. 5, 2013, pp. 1861 - 1864.

[45] E. Zitzler, L. Thiele, "An Evolutionary Algorithm for Multiobjective Optimization: The Strength Pareto Approach," Tech. Rep. 43, Comput. Eng. Networks Lab. (TIK), Swiss Federal Inst. Technol. (ETH), 1998.

[46] E. Dilettoso, N. Salerno, "A Self-Adaptive Niching Genetic Algorithm for Multimodal Optimization of Electromagnetic Devices", *IEEE Trans. Magn.*, vol. 42, n. 3, pp. 1203-1206, 2006.

[47] C. Magele et al., "Niching Evolution Strategies for Simultaneously Finding Global and Pareto Optimal Solutions", *IEEE Trans. Magn.*, vol. 46, n. 8, pp. 2743-2746, 2010.

[48] S. A. Rizzo, "Evolutionary Algorithms for Multi-Objective Optimization of Electromagnetic Devices, Ph. D. Thesis, Catania (Italy), 2010

[49] R. Hooke, T. A. Jeeves, "Direct search solution of numerical and statistical problems", Journal of the Association for Computing Machinery, 8, 1961, pp. 212-229.

[50] Torczon, V. (1997). On the convergence of pattern search algorithms. *SIAM Journal on Optimization*, 7(1):1-25.

[51] Torczon, V. and Trosset, M. W. (1997). From evolutionary operation to parallel direct search: Pattern search algorithms for numerical optimization. *Computing Science and Statistics*, 29.

[52] E. Dilettoso, S.A. Rizzo, N. Salerno, "SALHE-EA: a New Evolutionary Algorithm for Multi-Objective Optimization of Electromagnetic Devices", Intelligent Computer Techniques in Applied Electromagnetic, Springer-Verlag, Vol. 119, Berlin Heidelberg, 2008, pp. 37-45.

[53] S. Alfonzetti, E. Dilettoso, S. A. Rizzo and N. Salerno, "Stochastic optimization of magnetic shields in induction heating applications by means of the FEM-DBCI method and the SALHE evolutionary algorithm", *IEEE Trans. Magn.*, vol. 45, n. 3, pp. 1752-1755, 2009.

[54] M. Tomassini. Parallel and distributed evolutionary algorithms: A review. Evolutionary Algorithms in Engineering and Computer Science, ed. K. Miettinen ed al., J. Wiley and Sons, Chichester, 113-133, 1999.

[55] B.Sareni, L.Krahenbuhl and A. Nicolas, "Niching genetic algorithms for optimization in electromagnetics. I. Fundamentals", *IEEE Trans. on Evol. Comp.*, vol. 34, n.5, pp 2984-2987, 1998.

[56] P. Alotto, U. Baumgartner, F. Freschi, M. Jaindl, A. Kostinger, C. Magele, W. Renhart, M. Repetto "SMES Optimization Benchmark Extended: Introducing Uncertainties and Pareto Optimal Solutions into TEAM22", *IEEE Trans. on Magnetics,* vol. 44, no.6, pp. 106 -1069, 2008.

[57] T. Leuca, et.al. E. Vladu, M. Novac and O. Novac, "Induction heating optimal design by means of genetic algorithms", HES-07, Int. Sym. on Heating by Electromagnetic Sources, Padua, Italy, pp. 381-386, 2007.

[58] M. Chiampi et al, "Fuzzy Approach for Multiobjective Optimization in Magnetics" *IEEE Trans. on Magnetics*, 32, pp. 1234-1237, 1996.

[59] E. Dilettoso, S. A. Rizzo, N. Salerno, "A Parallel Version of the Self-Adaptive Low-High Evaluation Evolutionary-Algorithm for Electromagnetic Device Optimization", *IEEE Transactions on Magnetics*, vol. 50, n. 2, 2014, pp. 7015604_1-7015604_4. (PSALHE-EA algorithm available at http://wwwelfin.diees.unict.it/esg/research.phtml)